

1 Estimating the Thermodynamic Contribution of Post-Industrial 2 Warming to Recent Greenland Ice Sheet Surface Mass Loss

3 Jonathon R. Preece¹, Patrick Alexander^{2,3}, Thomas L. Mote¹, Gabriel J. Kooperman¹,
4 Xavier Fettweis⁴, and Marco Tedesco^{2,3},

5 ¹Department of Geography, University of Georgia, Athens, 30602, USA.

6 ²Lamont-Doherty Earth Observatory, Columbia University, Palisades, 10964, USA.

7 ³NASA Goddard Institute for Space Studies, New York, 10025, USA.

8 ⁴Laboratory of Climatology, Department of Geography, SPHERES research unit, University of Liège, Liège, Belgium

9
10 *Correspondence to:* Jonathon R. Preece (jonathon.preece@uga.edu)

11 **Abstract.** The pronounced increase in meltwater runoff from the Greenland Ice Sheet in recent decades represents an important
12 source of global sea-level rise. The role of anomalous anticyclonic circulation patterns in facilitating this increase has been
13 widely documented; however, this change in atmospheric circulation has coincided with a rapidly warming Arctic. While
14 amplified Arctic warming has undoubtedly contributed to trends in Greenland’s mass loss, the contribution of this shift in
15 background conditions relative to changes in regional circulation patterns has yet to be quantified. Here, we apply the pseudo-
16 global warming method of dynamical downscaling to estimate the contribution of the change in the thermodynamic
17 background state under global warming to observed Greenland Ice Sheet surface mass loss since the turn of the century. Our
18 analysis demonstrates that, had the 2000–2019 sequence of atmospheric circulation occurred under a preindustrial
19 thermodynamic background state, anomalous surface mass loss from the ice sheet would have been reduced by over 62%
20 relative to observations. We show that the change in the thermodynamic environment under amplified Arctic warming has
21 augmented melt of the ice sheet via longwave radiative effects accompanying an increase in atmospheric water vapor content.
22 Furthermore, the thermodynamic contribution to surface mass loss during the record melt years of 2012 and 2019 was less
23 than half that of the long-term average, suggesting that the pronounced mass loss during those two summers was more a result
24 of the anomalous atmospheric circulation than a direct consequence of the long-term warming trend.

25 1 Introduction

26 The Greenland Ice Sheet has undergone persistent mass loss since the turn of the century (Hanna et al., 2014, 2024; Khan et
27 al., 2015; Kjeldsen et al., 2015; Mouginito et al., 2019; Otosaka et al., 2023; The IMBIE Team et al., 2020; Velicogna et al.,
28 2020). While highly variable, mass loss from the Greenland Ice Sheet has consistently raised global mean sea level by over
29 0.5 mm yr⁻¹ in recent decades, contributing to sea-level rise at approximately twice the rate of the Antarctic Ice Sheet (Cazenave

30 et al., 2018; Horwath et al., 2022; Smith et al., 2020; The GlaMBIE Team et al., 2025; The IMBIE team et al., 2018; The
31 IMBIE Team et al., 2020). Estimates place the total contribution of Greenland at over 10 mm of sea level rise since the 1990s
32 (Mouginot et al., 2019; The IMBIE Team et al., 2020). Moreover, most of the impact of recent climate change on total mass
33 balance has yet to be realized, as the timescale at which ice sheet dynamics adjust to a climate perturbation is an order of
34 magnitude or greater than that of the surface mass balance (SMB) response (Box et al., 2022). Recent work conservatively
35 estimates another ~274 mm of committed sea level rise before the ice sheet achieves balance with the current climate state—
36 i.e., even without considering the additional impact of any future warming scenario (Box et al., 2022).

37
38 Over Greenland, there has been both an increase in solid-ice discharge and a decline in SMB over the past few decades (van
39 den Broeke et al., 2009a; Mankoff et al., 2019; The IMBIE Team et al., 2020); however, increased runoff has caused SMB to
40 decline at a rate twice that of the observed increase in dynamic ice loss (Box et al., 2022; Fettweis et al., 2017, 2020; Mote,
41 2007; Noël et al., 2017). Consequently, SMB reductions have surpassed discharge as the largest source of mass loss (Mouginot
42 et al., 2019) and, according to dynamically downscaled CMIP5 and CMIP6 global climate model (GCM) output, SMB losses
43 are projected to exceed mass accumulation on their own by the year 2100 unless the most ambitious mitigation efforts are
44 implemented (Noël et al., 2021). This timeline, however, contains considerable uncertainty as differences in prescribed bare-
45 ice albedo and firn model parameterizations have been shown to yield a twofold spread in simulated runoff between the three
46 leading polar Regional Climate Models (RCMs) under a common future radiative forcing, with RACMO – the RCM used to
47 derive this estimate – underestimating future runoff relative to HIRHAM and MAR (Glaude et al., 2024).

48
49 This change in ice sheet surface conditions has been associated with a recent shift in summer atmospheric circulation over the
50 North Atlantic. The decline in SMB has coincided with a more persistently negative North Atlantic Oscillation (NAO) and an
51 increase in atmospheric blocking episodes over Greenland (Bevis et al., 2019; Fettweis et al., 2013; Hanna et al., 2015, 2016,
52 2018b, 2022; Hofer et al., 2017). Indeed, previous studies have shown a statistically significant increase in summer Greenland
53 blocking between the 1990's and early 2010's using a variety of blocking detection methods (Davini and D'Andrea, 2020;
54 Hanna et al., 2022; Lee and Polvani, 2026; Luu et al., 2024; Woollings et al., 2018). While multi-year mean summer Greenland
55 blocking frequency has declined since its peak around 2010, interannual variability has remained anomalously high with
56 extreme blocking episodes again facilitating record-setting melt of the ice sheet in 2019 and 2023 (Bonsoms et al., 2026;
57 Cullather et al., 2020; Lee and Polvani, 2026; Luu et al., 2024; Tedesco and Fettweis, 2020). More frequent blocking has
58 played a key role in encouraging melt via multiple contrasting mechanisms. The increase in surface melt has been ascribed to
59 the suppression of cloud cover by large-scale subsidence within the blocking ridge (Hofer et al., 2017). This reduction in cloud
60 cover has allowed for anomalously high downward shortwave radiation over the southern ice sheet which, owing to its lower
61 surface albedo, is more sensitive to changes in shortwave radiation than other regions of the ice sheet (Hofer et al., 2017; Wang
62 et al., 2019). Other studies, however, have demonstrated the importance of cloud longwave radiative effects, particularly in
63 regions where albedo is high, such as the northern ice sheet and over the high-elevation accumulation zone (Gallagher et al.,

64 2018; Lenaerts et al., 2019; Noël et al., 2019; Orsi et al., 2017; Wang et al., 2019). Southerly moisture transport upstream of a
65 blocking anticyclone in July 2012 supported the formation of low-level cloud cover that produced melt over the highest
66 elevations of the ice sheet for the first time in over a century (Bennartz et al., 2013; Clausen et al., 1988; Fausto et al., 2016b,
67 a; Mattingly et al., 2018; Meese et al., 1994; Neff et al., 2014; Nghiem et al., 2012). Additionally, the high-amplitude Omega
68 blocking patterns that have increased most in recent summers deliver moisture farther poleward, generating above-normal
69 downward longwave radiation over northern Greenland (Preece et al., 2022)—conditions which have caused pronounced
70 growth of the ablation zone and spurred a disproportionate increase in runoff from the northern drainages of the ice sheet (Noël
71 et al., 2019).

72

73 A natural question is whether this shift in summer circulation may be a symptom of climate change. At the hemispheric scale,
74 there are several theoretical frameworks that postulate a link between changes in the meridional temperature gradient under
75 Arctic Amplification and more frequent persistent weather extremes (Cohen et al., 2014; Coumou et al., 2018; Francis and
76 Vavrus, 2012), and there is mounting evidence of such a link during summer (Cattiaux et al., 2016; Coumou et al., 2015; Di
77 Capua and Coumou, 2016; Kornhuber and Tamarin-Brodsky, 2021; Vavrus et al., 2017). However, not only have GCMs failed
78 to capture the positive trend in Greenland blocking, they consistently predict a decline in blocking frequency in the region
79 (Delhasse et al., 2021; Hanna et al., 2018a)—a critical source of uncertainty regarding a causal link between anthropogenic
80 climate change and the observed shift in summer circulation over Greenland. Conversely, the change in the background
81 thermodynamic environment, and its resulting impact on SMB represents a more robust signal of climate change than the
82 potential dynamical response outlined above. Multiple well-documented radiative feedbacks have helped warm the Arctic at
83 four times the global average rate (Pithan and Mauritsen, 2014; Rantanen et al., 2022; Serreze and Barry, 2011). This
84 constitutes a likely contributor to the nonlinear decline in SMB, as surface melt would be expected to increase in frequency
85 and magnitude in a warmer, more humid atmosphere.

86

87 The thermodynamic environment over Greenland is surely influenced by changes occurring more broadly throughout the
88 Arctic. Indeed, Box et al. (2013) linked increased precipitation over Greenland to higher Northern Hemisphere surface air
89 temperature and showed that this statistical relationship was more robust than when considering local near-surface
90 temperatures over Greenland or North Atlantic SST—a result that emphasizes the importance of remotely-sourced heat and
91 moisture to the SMB. However, local sea-surface conditions (SSCs) may also play an important role. Specifically, sea ice
92 reductions over adjacent waters could further contribute to elevated temperatures over Greenland through the water vapor
93 feedback, wherein a warmer atmosphere together with an ice-free ocean increases atmospheric water vapor, which then
94 enhances longwave radiative forcing at the surface (Pithan and Mauritsen, 2014; Trenberth, 2011). One of the more intuitive
95 ways that sea ice loss could impact the ice sheet is through advection of warm, moisture-enriched air from the neighboring
96 seas. Studies have revealed a relationship between changes in sea-ice concentration near Greenland and ice sheet SMB
97 (Pedersen and Christensen, 2019; Rennermalm et al., 2009); however, these studies fail to separate direct marine influence

98 from any indirect effects via alteration of the large-scale circulation by oceanic thermal forcing (Ballinger et al., 2019; Liu et
99 al., 2016) or relationships that might arise as a byproduct of mutual forcing of local sea ice concentration (SIC) and ice sheet
100 melt by the large-scale synoptic setting (Ballinger et al., 2018; Stroeve et al., 2017).

101
102 Several modeling efforts have demonstrated minimal contribution from local SSCs during summers of pronounced melt due
103 to the persistent katabatic outflow over the ice sheet that acts as a barrier to onshore advection (Hanna et al., 2009, 2014; Noël
104 et al., 2014); however, observational evidence suggests that local SSCs may play an important role earlier in spring. While
105 melt events during summer and fall are primarily a product of large-scale atmospheric conditions (Ballinger et al., 2019;
106 Hermann et al., 2020; Noël et al., 2014), recent work demonstrated elevated atmospheric moisture and enhanced downward
107 longwave radiation over the ice sheet approximately one week following sea ice retreat in the Baffin Bay and Davis Strait in
108 years of early melt, suggesting that local sea ice anomalies precondition the ice sheet for early melt onset (Stroeve et al., 2017).

109
110 Disentangling the relative contributions of atmospheric dynamics versus thermodynamics is an intractable problem using
111 observations alone. Previous studies have utilized RCMs to examine the sensitivity of the SMB to perturbations in SSCs
112 (Hanna et al., 2009, 2014; Noël et al., 2014) or atmospheric thermodynamic fields (Delhasse et al., 2018); however, none of
113 these efforts examined the combined influence of atmospheric and SSCs. Furthermore, these studies either applied arbitrary
114 perturbations to the targeted boundary fields or examined a single melt season and, therefore, did not aim to measure the
115 existent contribution of observed changes in these fields to mass loss.

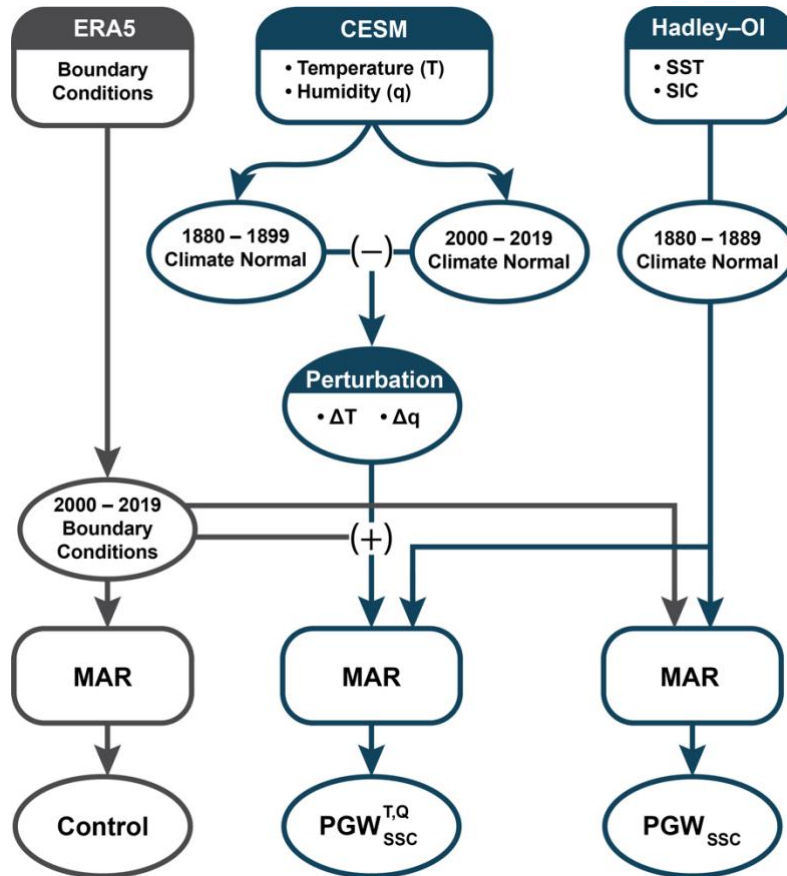
116
117 Here, we provide an estimate of the relative contributions of dynamical versus thermodynamic change to recent Greenland ice
118 sheet surface mass loss using the pseudo-global warming (PGW) method of dynamical downscaling. The PGW method uses
119 adjusted reanalysis data for the initial and lateral boundary conditions of an RCM (Kawase et al., 2008; Kimura and Kitoh,
120 2007; Schär et al., 1996). To obtain the adjusted boundary conditions, this method applies a climate change perturbation signal
121 that is estimated from GCM output by assuming a linear change in the boundary fields between the control period (i.e., the
122 period of observed reanalysis data) and some alternative period of interest with a contrasting thermodynamic background state
123 (Kawase et al., 2008; Rasmussen et al., 2011; Schär et al., 1996). Thus, the PGW technique effectively isolates the impact of
124 the long-term thermodynamic component of climate change by assuming that the timing and structure of synoptic disturbances
125 along the RCM's boundaries will be the same in the alternative period as during the control (Lackmann, 2015).

126
127 While the PGW method is typically utilized to simulate future conditions, it can also be used to investigate how recent periods
128 of climate or individual weather events would have behaved under past conditions. For example, Lackmann (2015) estimated
129 the thermodynamic contribution of recent climate change to the evolution of Hurricane Sandy by comparing a control run to a
130 PGW simulation using boundary conditions that were adjusted to reflect the climate of the late 19th Century. Likewise, Kawase
131 (2008) used a similar approach in a climate change attribution study of the Mei-yu rain band in southern China. Here we use

132 the PGW method to quantify what the magnitude of surface melt would have been if the recent dynamical forcing of the ice
 133 sheet had occurred in a preindustrial thermodynamic background state by answering the following questions: (1) How much
 134 of the recent SMB decline can be attributed to the combined influence of increasing background temperatures and contributions
 135 from local SSCs? (2) What portion of the thermodynamic influence is due to adjacent SSC change alone and do SSCs have a
 136 discernible impact on the timing or duration of the melt season?

137 2. Experimental Design

138 A model schematic outlining our approach is presented as Figure 1. Atmospheric conditions and the SMB and surface energy
 139 balance (SEB) response were modeled using the RCM, Modèle Atmosphérique Régional (MAR) (Fettweis et al., 2005, 2020;
 140 Lefebvre et al., 2005). MAR includes a surface-atmosphere energy and mass transfer scheme with a one-dimensional snowpack
 141 model that represents snow grain metamorphism and its impact on albedo, and accounts for the percolation and refreeze of
 142 meltwater within the snowpack (Amory et al., 2021; Brun et al., 1989, 1992). For a more detailed description of MAR, see
 143 Amory *et al.* (2021). Here, we employed MAR version 3.12 initialized and forced at its lateral boundaries with 6-hourly ERA5
 144 reanalysis data and integrated over a 120x180, 20-km grid with 24 vertical atmospheric levels.



145 **Figure 1. Model experiment overview.** Model schematic illustrating the design of the control run (gray outlines) and pseudo-global
146 warming experiments (blue outlines). For the control run, all boundary fields including SSCs were sourced from ERA5. In $PGW_{SSC}^{T,Q}$, the
147 atmospheric thermodynamic fields of air temperature (T) and specific humidity (Q) from ERA5 were adjusted to reflect preindustrial
148 conditions by applying a climate change perturbation signal derived from Community Earth System Model (CESM) data, and preindustrial
149 SSCs of SST and SIC were prescribed using merged Hadley-OI observational data. In PGW_{SSC} , only SST and SIC were altered to reflect
150 preindustrial conditions.
151

152 As a control, we forced MAR with ERA5 data spanning 2000 to 2019 to represent historical conditions during the recent period
153 of anomalous Greenland blocking (Figure 1, gray components). For the control, all boundary fields including the SSCs of sea-
154 surface temperature (SST) and SIC were sourced from ERA5. To simulate the preindustrial thermodynamic state (Figure 1,
155 blue components), we adjusted the boundary conditions of air temperature and specific humidity using perturbations obtained
156 from the NCAR Community Earth System Model-Large Ensemble (CESM-LE) project (Kay et al., 2015), while zonal and
157 meridional winds at the model boundaries were left unaltered to minimize differences in the large-scale atmospheric circulation
158 between the experiment and the control. For the pre-industrial simulations, we adjusted ERA5 air temperature and specific
159 humidity using a climate change perturbation derived from the 40 ensemble members of the NCAR CESM-LE project as
160 follows:
161

$$\Delta x = \underline{x}_p - \underline{x}_c$$

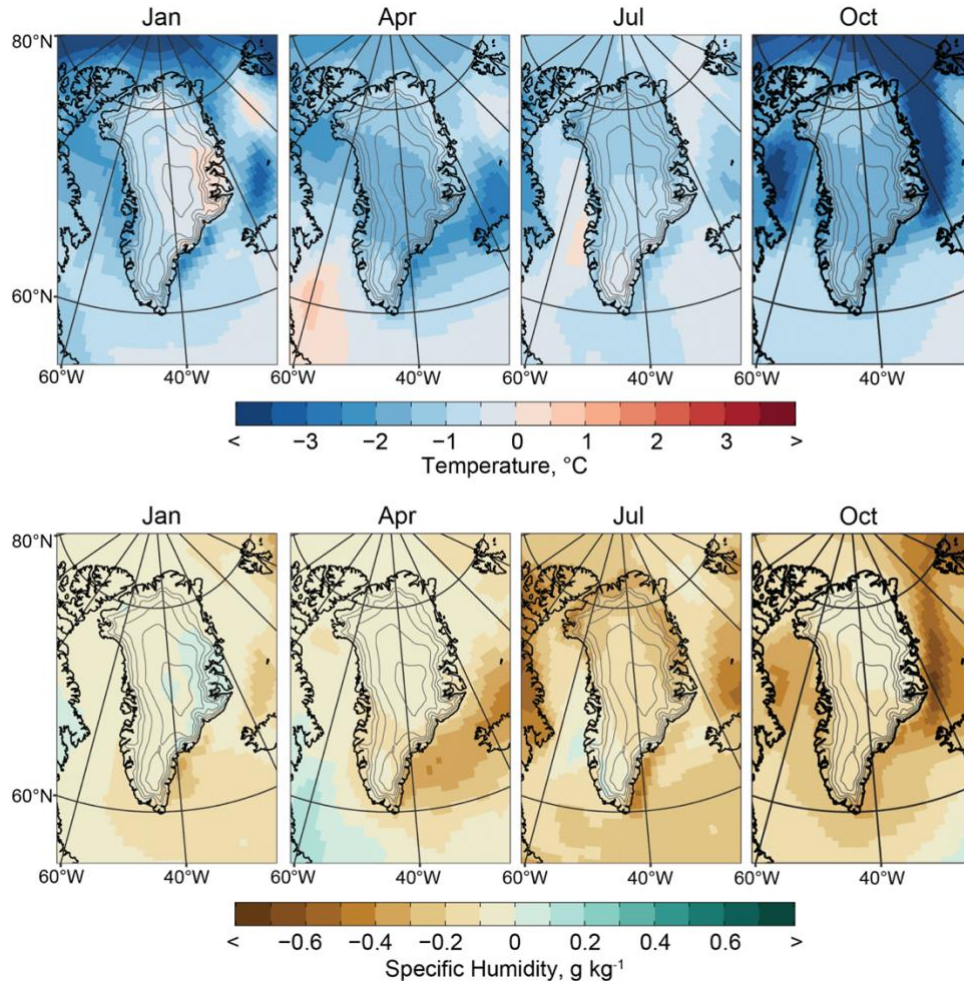
162
163
164 Where Δx is the climate change perturbation for variable x , \underline{x}_p is the ensemble-averaged, long-term monthly mean of variable
165 x for a preindustrial reference period of 1880–1899, and \underline{x}_c is the ensemble-averaged, long-term monthly mean of variable x
166 for a control period of 2000–2019. We then linearly interpolated the monthly climate change perturbations derived from
167 CESM-LE temporally to a 6-hourly timestep, vertically to ECMWF’s L137 hybrid sigma-pressure levels, and horizontally to
168 the ERA5 grid before adding them to the corresponding ERA5 boundary fields that were used to force MAR. A comparison
169 of 500 hPa geopotential height over the study area shows strong temporal covariability between simulations, indicating that
170 the large-scale circulation of the control was well preserved in our application of the PGW method (Fig. S1).
171

172 While GCMs aim to capture the periodicity of internal climate variability, they may not accurately resolve the magnitude of
173 said variability and the precise timing of a particular mode of variability differs between individual ensemble members.
174 Considering a single GCM simulation alone would risk enhancing or suppressing the magnitude of the climate perturbation
175 signal if the control and alternative periods are characterized by opposing phases of a relevant mode of internal variability. For
176 example, an anomalously negative summer NAO since the turn of the century has favored the advection of warm, moist air
177 over Greenland (Fettweis et al., 2013; Hanna et al., 2013; Henderson et al., 2021; Mattingly et al., 2018; Mote, 1998; Tedesco
178 et al., 2016). Since our intent is to isolate the contribution of background thermodynamic change to mass loss, deriving a
179 perturbation signal from observations would overestimate the baseline change in temperature and humidity around Greenland
180 because it would also include the dynamical contribution of an anomalously negative NAO during our control period. Taking

181 an ensemble mean of the CESM-LE effectively removes the noise of internal climate variability by averaging across the
182 differing phases resolved by each ensemble member for a given date, thereby providing a more appropriate estimate of the
183 change in the mean climate state.

184

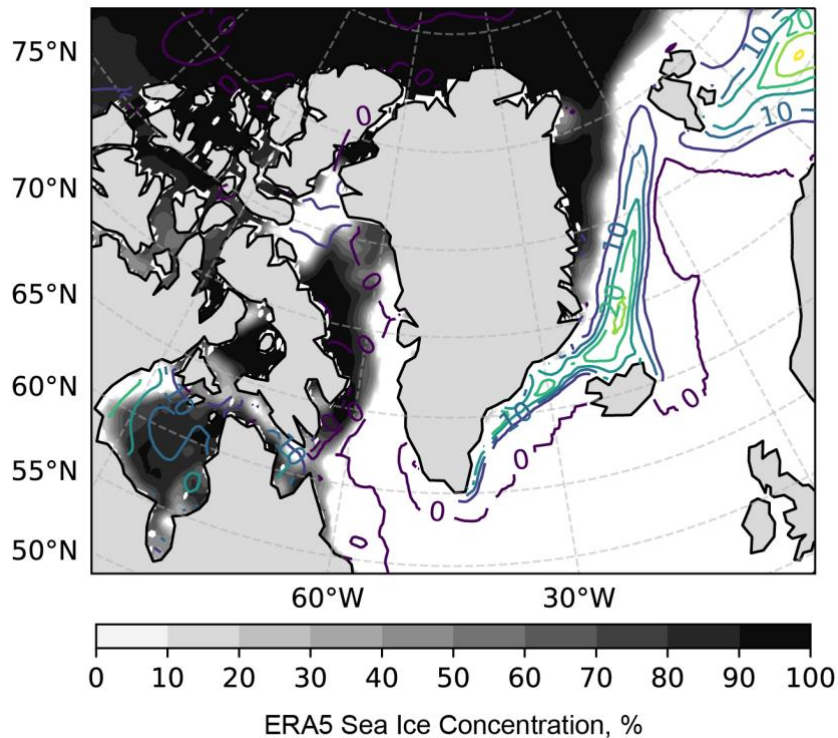
185 Figure 2 shows a subset of the monthly surface air temperature and specific humidity perturbation fields that were applied at
186 the lateral boundaries of MAR. Seasonally, CESM-LE simulates the greatest temperature difference in fall and winter (Fig. 2,
187 top row), consistent with what should be expected under Arctic amplification, which is largely driven by sea ice loss (Screen
188 and Simmonds, 2010). Differences in near-surface atmospheric moisture are largely reflective of the Clausius-Clapeyron
189 relation, with drier conditions mirroring locations of cooler temperatures in the preindustrial climate (Fig. 2, bottom row).



190 **Figure 2. Climate change perturbation fields.** Perturbation fields derived from CESM-LE for surface air temperature (top row) and specific
191 humidity (bottom row) shown for a selection of months equally spaced throughout the year as labeled at the top of each panel. Perturbation
192 fields shown for the lowermost model level after vertically interpolating to the same ECMWF L137 hybrid sigma-pressure levels as the
193 ERA5 boundary conditions. Contour interval: 500 m. Range: 1000–3000 m.

194

195 The use of a GCM-derived perturbation signal presents issues when dealing with sea ice. The change in SIC is greatest along
196 the sharply defined sea ice front and the GCM's representation may not geographically align with observations. Figure 3
197 presents one such comparison for June 15, 2018, which occurs during a month of exceptionally low SIC in the Greenland Sea.
198 There is a considerable gap between the observed sea ice front and area of greatest SIC change according to CESM-LE,
199 such that the application of this perturbation signal would result in a locally high SIC stretching from Iceland to Svalbard that is
200 separated from the main body of sea ice. To avoid this unrealistic distribution, and to ensure consistency between SIC and
201 SST, we prescribed both SIC and SST in our experimental simulations using 1880–1899 long-term monthly means calculated
202 from the merged Hadley-OI observational dataset (Shea et al., 2020) and interpolated to a 6-hourly timestep.



203 **Figure 3. Sea ice representation.** Comparison of observed sea ice concentration on June 15, 2018 (shading) and the corresponding CESM-
204 LE climate perturbation signal (contours, 5% interval).
205

206 Contrary to global SST trends, there are extensive areas around Greenland where SST during the preindustrial period was
207 higher than during the current period (Figure S2). This is most apparent during winter and spring when higher preindustrial
208 SST is observed throughout the northern subpolar gyre to the southeast of Greenland and extending from the southern
209 Greenland coast along the sea ice edge to Svalbard. The spatial and seasonal pattern of lower SST since the preindustrial period
210 matches the fingerprint of the so-called North Atlantic warming hole—an observed decrease in subpolar North Atlantic SST
211 that has been attributed to a weakening of the Atlantic meridional overturning circulation and associated poleward oceanic

212 heat transport as a consequence of climate change (Caesar et al., 2018). In summer, SST throughout much of the region was
213 lower during the preindustrial period (Figure S2).

214

215 After interpolating the Hadley-OI fields to a 6-hourly timestep, we applied the following adjustments based on the work of
216 Hurrell *et al.* (2008) to further ensure consistency between SST and SIC:

- 217 • If an interpolated grid cell had a SIC > 90%, we set the SST of that cell to the sea ice freezing point of -1.8 °C.
- 218 • Where 15% < SIC < 90% we adjusted SST as follows:

$$219 \text{ SST} = 9.328(0.729 - (\text{SIC}/100)^3) - 1.8, \quad (1)$$

- 220 • SIC was set to zero if SST > 4.97 °C.
- 221 • Where -1.8 °C < SST < 4.97 °C we adjusted SIC as follows:

$$222 \text{ SIC} = 100(0.729 - (\text{SST} + 1.8)/9.328)^{\frac{1}{3}}, \quad (2)$$

223

224 Following Noël et al. (2014), we allotted 5 years of spin-up time for each model simulation to allow the MAR snowpack model
225 to adjust to the altered boundary conditions. In $PGW_{SSC}^{T,Q}$, we adjusted the boundary forcing fields of temperature (T), specific
226 humidity (Q), and the SSCs of SST and SIC to reflect the long-term preindustrial conditions. Thus, by comparing $PGW_{SSC}^{T,Q}$ to
227 the control, we quantify the thermodynamic contribution to recent surface mass loss. For PGW_{SSC} , we adjusted SST and SIC
228 to reflect preindustrial conditions, while leaving the temperature and humidity fields unaltered. ~~to~~ ^{to} quantify the portion of
229 recent surface mass loss that is due to changes in local SSCs

230

231 The design of PGW_{SSC} also allows us to test how much of the mechanism identified by Stroeve *et al.* (2017) – that low spring
232 SIC in the seas surrounding Greenland preconditions the ice sheet for melt in early melt onset years – is due to direct
233 thermodynamic forcing alone. Following Stroeve *et al.* (2017), we define melt onset as the first instance of five or more
234 consecutive days of melt. The date of freeze onset is then defined as the first day following the last instance of five or more
235 consecutive days of melt. We calculated all measures of the melt season at each MAR grid pixel, then tested for significant
236 differences between the PGW simulations and the control using a paired Wilcoxon signed-rank test (Wilcoxon, 1945) with a
237 predetermined significance level of $\alpha = 0.05$ (i.e., 95 % confidence level).

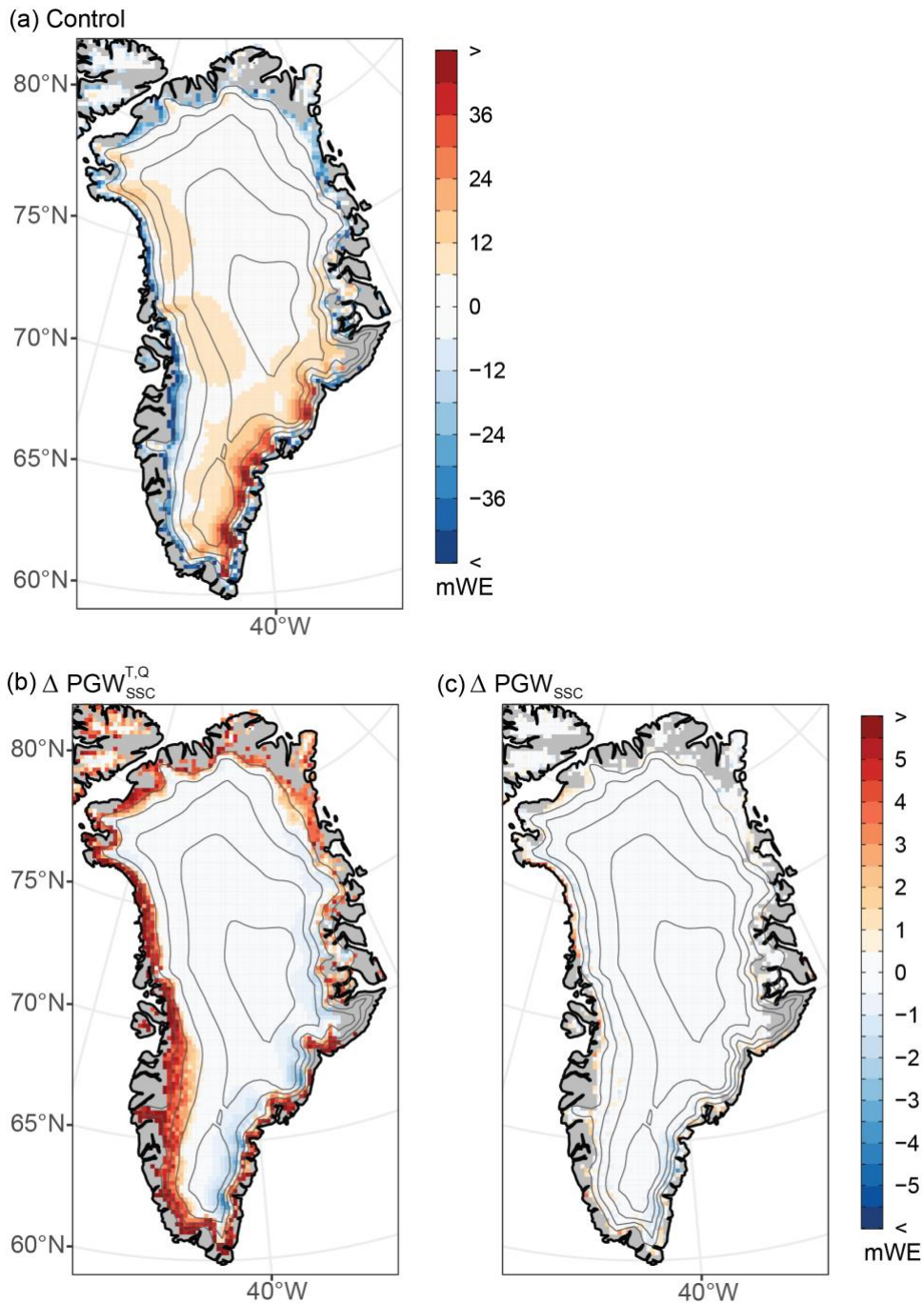
239 3.1. Thermodynamic Contribution to SMB Change

240 Figure 4 presents a comparison of the cumulative SMB anomaly between the control run and each PGW simulation. The
 241 control run (Fig. 4, gray line) shows a cumulative SMB anomaly of -1852 Gt over the study period of 2000 to 2019, congruent
 242 with other estimates (IMBIE, 2020), and corresponding to approximately 5 mm of global sea level rise. A gradual shift to a
 243 negative cumulative SMB occurs around 2005, coinciding with the transition to a more persistently negative NAO and rise in
 244 Greenland blocking frequency (Hanna et al., 2015; Hofer et al., 2017). The first instance of pronounced mass loss is evident
 245 as a sharp decrease in 2007—a year of unprecedented surface melt up to that point in the satellite record (Mote, 2007). The
 246 exceptional melt years of 2012 (Hanna et al., 2014; Nghiem et al., 2012) and 2019 (Cullather et al., 2020; Hanna et al., 2021;
 247 Tedesco and Fettweis, 2020) are readily apparent as drops in the control time series.



248 **Figure 4. Temporal evolution of the SMB under contrasting thermodynamic background conditions.** Shown are the cumulative SMB
 249 anomaly time series for the control (gray), $PGW_{SSC}^{T,Q}$ (blue dashed), and PGW_{SSC} (green dashed) simulations. Anomalies calculated with
 250 respect to the 1980-1989 reference period. Left axis shows cumulative SMB anomaly; right axis shows the equivalent sea-level contribution.
 251 Annotations detail the difference in the final cumulative SMB between each of the PGW simulations and the control.
 252

253 Comparing the control with $PGW_{SSC}^{T,Q}$ (Fig. 4, blue dashed line) highlights the substantial thermodynamic contribution to the
 254 recent change in SMB. A difference in cumulative SMB between the two simulations of 1145 Gt amounts to a 62% reduction
 255 in surface mass loss in $PGW_{SSC}^{T,Q}$ relative to the control. Under the preindustrial thermodynamic setting of $PGW_{SSC}^{T,Q}$, the ice sheet
 256 maintains a positive SMB anomaly through 2009, and the mass loss for each melt season is reduced relative to the control.
 257 This holds true for the exceptional melt years of 2012 and 2019; however, while the magnitude of mass loss is greater when
 258 the warming signal is included, the relative contribution of those individual melt seasons to the total SMB change over the 20-
 259 year period is greater for $PGW_{SSC}^{T,Q}$ —In a preindustrial climate, 2012 and 2019 each account for ~250 Gt of mass loss, which –
 260 combined – is approximately 2/3 of the total mass loss in $PGW_{SSC}^{T,Q}$ (Fig. 4). Furthermore, while the rate of mass loss is reduced
 261 from 2013 to 2018 in the control, this period undergoes a slight surface mass gain in $PGW_{SSC}^{T,Q}$.



262 **Figure 5. Spatial distribution of SMB change under contrasting thermodynamic background conditions.** (a) The cumulative SMB
 263 anomaly over the full study period of 2000–2019 as represented by the control simulation. (b) $PGW_{SSC}^{T,Q}$ cumulative SMB minus the control.
 264 (c) PGW_{SSC} cumulative SMB minus the control. Contour interval: 500 m. Range: 1000–3000 m.
 265

266 The cumulative SMB anomaly in PGW_{SSC} (Fig. 4, green dashed line) is 105 Gt greater than that for the control. This relatively
267 small difference indicates that there has been minimal direct thermodynamic influence by changes in local SST and SIC over
268 the study period—a result that is consistent with previous modeling studies which showed low SMB sensitivity when applying
269 arbitrary perturbations to local SSCs (Hanna et al., 2009, 2014; Noël et al., 2014), adding confidence that changes occurring
270 more widely throughout the Arctic and sub-Arctic dominate the thermodynamic contribution to mass loss.

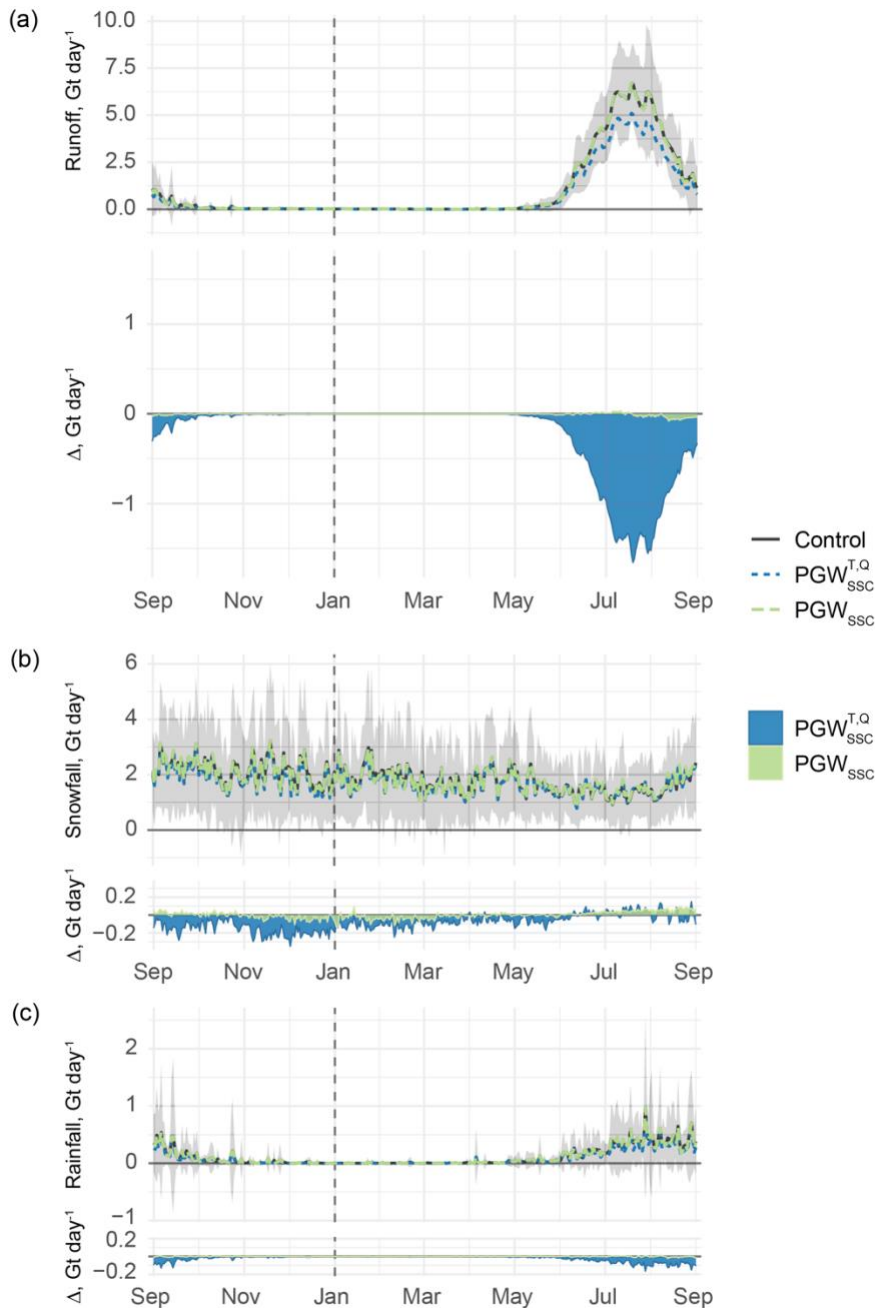
271
272 The cumulative SMB over the study period in the control (Fig 5a) shows a band of negative SMB along the perimeter of the
273 ice sheet that demarcates the ablation zone. The greatest accumulation occurs along the southeast coast of Greenland and is a
274 product of orographic enhancement of precipitation associated with lee-side cyclones that form in westerly flow over southern
275 Greenland (Bromwich et al., 1998; Rogers et al., 2004; Schuenemann et al., 2009). Other areas of notable SMB gains include
276 west and northwest Greenland. Snow accumulation in these areas is fueled by bouts of intense water vapor transport through
277 the Davis Strait that have increased in frequency in recent decades (Mattingly et al., 2016, 2018).

278
279 Relative to the control, $PGW_{SSC}^{T,Q}$ yields a greater cumulative SMB in a band that stretches around the perimeter of the ice sheet,
280 exceeding 2000 m elevation in some locations in southwest Greenland (Fig 5b)—a consequence of decreased meltwater runoff
281 in the preindustrial setting (Fig. S3a). At higher elevations over much of eastern Greenland and to a lesser extent over the
282 northwest ice sheet, a reduction in snowfall in the cooler and dryer atmosphere of $PGW_{SSC}^{T,Q}$ results in a lower SMB compared
283 to the control (Fig 5b, Fig. S3b). This represents a competing influence on SMB, as the same bouts of remotely sourced heat
284 and moisture that promote melt at lower elevations can also deliver anomalous snow accumulation over high elevations,
285 thereby offsetting SMB losses directly, through increased mass gains, and indirectly, by increasing the surface albedo (Bailey
286 and Hubbard, 2025; Mattingly et al., 2018).

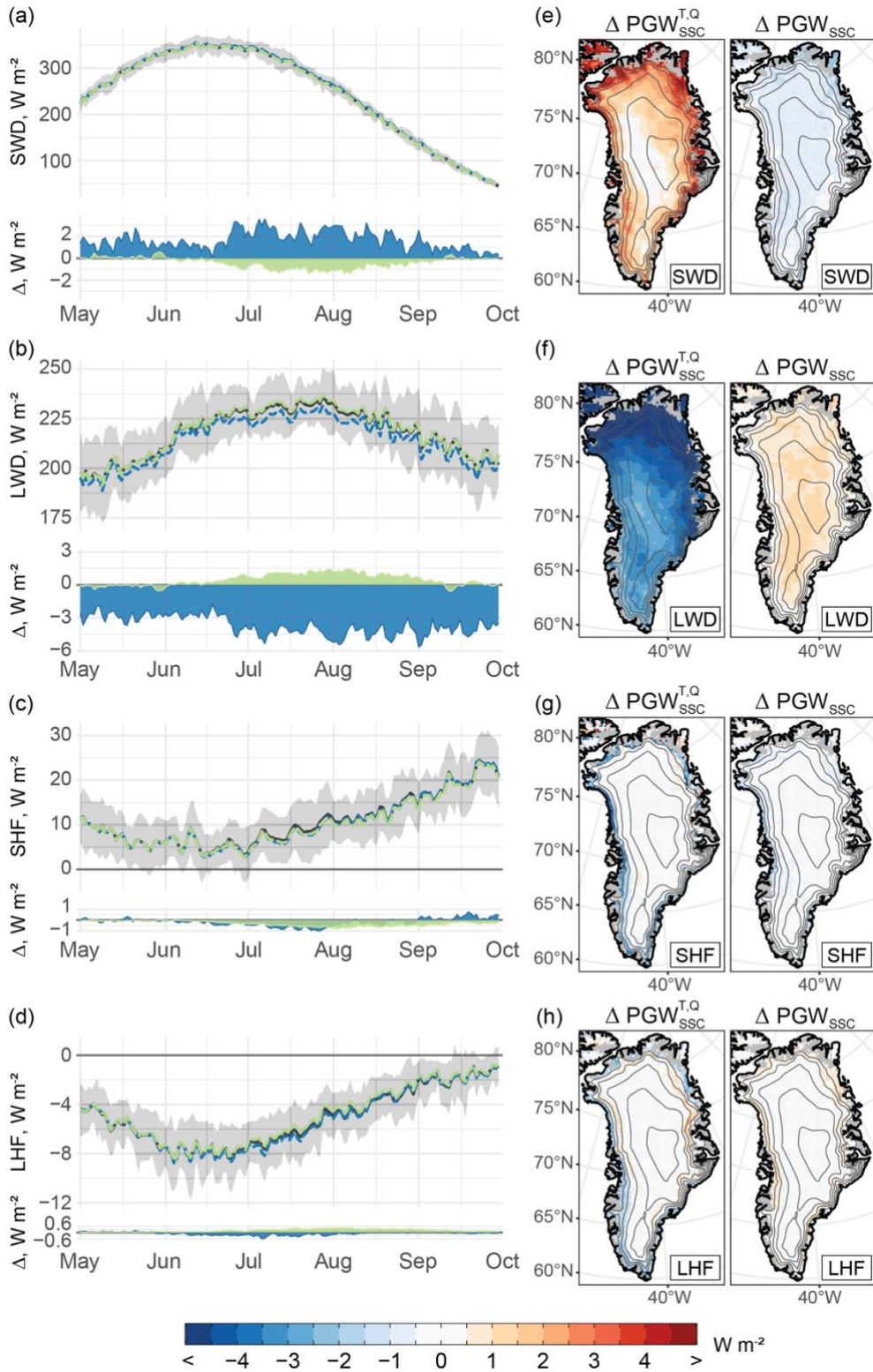
287
288 The greatest differences in surface runoff between $PGW_{SSC}^{T,Q}$ and the control are centered on mid-to-late July (Fig. 6a). Runoff
289 during the peak of the melt season in $PGW_{SSC}^{T,Q}$ was nearly 1 std. dev. below what has been typical since the turn of the century
290 (Fig 6a). The relative mass loss over high elevations evident in Fig 5b is driven by a reduction in snowfall throughout the cool
291 season; however this impact on snow accumulation is most apparent in fall and early winter when the greatest change in
292 background conditions have occurred (Fig. 2, 6b) (Serreze and Barry, 2011). In contrast with the rest of the year, there is a
293 slight increase in summer snowfall in $PGW_{SSC}^{T,Q}$ that coincides with a reduction in rainfall (Fig. 6c), consistent with the historical
294 record which shows greater partitioning toward liquid precipitation as the atmosphere has warmed in recent decades (Box et
295 al., 2023; van den Broeke et al., 2016).

296
297 The differences between PGW_{SSC} and the control show a similar pattern as observed for $PGW_{SSC}^{T,Q}$; however, they are
298 comparatively minimal in both magnitude and scale (Fig 5c). The change in SSCs reduces meltwater runoff resulting in higher

299 SMB (Fig 5c, Fig. S3d); however, this response is largely confined to grid cells along the periphery of the ice sheet. The isolated
300 impact of SSCs on snowfall is most evident along the southeast margin of the ice sheet and above ~1000 m in northwest
301 Greenland. Whereas runoff was diminished throughout the entire melt season $PW_{SSC}^{T,Q}$, the impact of SSCs alone on surface
302 melt emerges later (Fig. 6a), likely reflecting the stronger coupling between ocean and atmosphere as the thermal gradient
303 between them increases into the fall (Screen, 2017).



304 **Figure 6. Seasonal evolution of the SMB under contrasting thermodynamic background conditions.** Panels depict the seasonal
 305 progression of three principal SEB components: (a) Surface runoff, (b) snowfall, (c) rainfall. Top portion of each panel shows 2000–2019
 306 long-term daily mean totals of each SMB component throughout the melt season for the control (gray), $PGW_{SSC}^{T,Q}$ (blue dashed), and PGW_{SSC}
 307 (green dashed) simulations. Time series represent the spatially integrated sum of a given variable over the entire ice mask. Gray shading
 308 shows the 1σ range about the mean for the control simulation. Bottom portion shows the difference between each PGW simulation ($PGW_{SSC}^{T,Q}$,
 309 blue; PGW_{SSC} , green) and the control ($\Delta = PGW - \text{Control}$). The scale of the y-axis on the bottom portion is kept constant across all panels
 310 to facilitate comparison between SMB terms.



312 **Figure 7. The SEB of the Greenland Ice Sheet during the melt season under contrasting thermodynamic background conditions.** (a–
313 d) Top portion of each panel shows the 2000–2019 long-term daily mean values of each SEB component throughout the melt season for the
314 control (gray), $PGW_{SSC}^{T,Q}$ (blue dashed), and PGW_{SSC} (green dashed) simulations. Time series represent the spatial average taken over the
315 entire ice mask for a given variable. Gray shading shows the 1σ range about the mean for the control simulation. Bottom portion shows the
316 difference between each PGW simulation ($PGW_{SSC}^{T,Q}$, blue; PGW_{SSC} , green) and the control ($\Delta = PGW - \text{Control}$). The scale of the y-axis on
317 the bottom portion is kept constant across all panels to facilitate comparison between SEB terms. (e–f) Maps depicting the difference between
318 the 2000–2019, Jun–Aug long-term mean of each SEB component between each PGW simulations ($PGW_{SSC}^{T,Q}$, left; PGW_{SSC} , right) and the
319 control. SEB components are organized by row: (a, e) downward shortwave radiation (SWD); (b, f) downward longwave radiation (LWD);
320 (c, g) sensible heat flux (SHF); (d, h) latent heat flux (LHF). Contour interval: 500 m. Range: 1000–3000 m.
321

322 While a decrease in snowfall relative to the control in the PGW simulations partially compensates for the relative mass gains
323 at lower elevations, the reduction in meltwater runoff is the primary determinant of the differences in cumulative SMB
324 observed in Fig. 4. Recognizing this, the next section focuses on the extended melt season to better understand the mechanisms
325 by which thermodynamic change has dictated surface runoff.

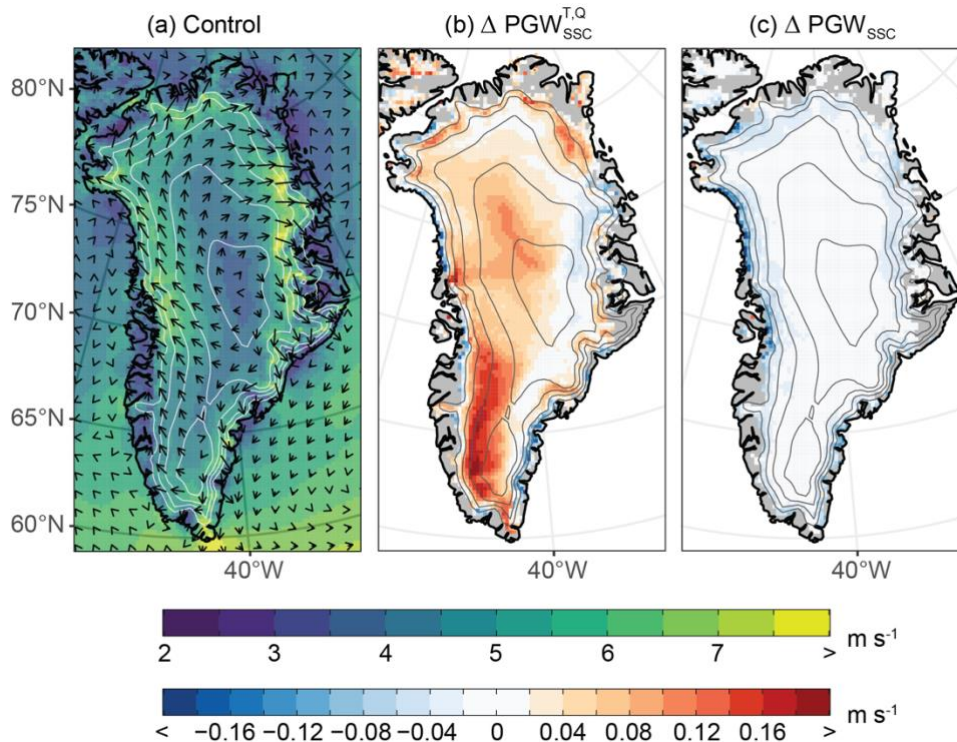
326 3.2. Thermodynamic Drivers of Surface Runoff

327 The preindustrial thermodynamic state of $PGW_{SSC}^{T,Q}$ is associated with an increase in downward shortwave radiation (SWD)
328 (Fig. 7a, e) and a decrease in downward longwave radiation (LWD) (Fig. 7b, f) throughout the melt season. The differences
329 between the control and $PGW_{SSC}^{T,Q}$ are greatest over the northern ice sheet, consistent with the thermodynamic signature in the
330 free atmosphere where the differences in both temperature and specific humidity at 600 hPa are maximized over northern
331 Greenland (Fig. S4). Turbulent fluxes are generally diminished in $PGW_{SSC}^{T,Q}$ relative to the control (Fig 7c,d) and differences
332 are focused along the outer margins of the ice sheet, where lower elevations display a decrease in both sensible (SHF) and
333 latent heat flux (LHF) in $PGW_{SSC}^{T,Q}$ that is mirrored by differences of the opposite sign over higher elevations (Fig. 7g, h).
334

335 The juxtaposition in the response of the turbulent fluxes in $PGW_{SSC}^{T,Q}$ appears to arise from opposing direct and indirect responses
336 to the change in background conditions. Along the ice sheet margins, a decrease in both SHF and LHF is consistent with a
337 direct reduction in the flux of heat and moisture to the surface of the ice sheet in a colder, drier preindustrial atmosphere.
338 Conversely, above normal turbulent fluxes over higher elevations follow indirectly from changes in the near-surface wind
339 field. Lower water vapor content in $PGW_{SSC}^{T,Q}$ (Fig. 2) reduces the longwave emissivity of the atmosphere, which would act to
340 lower surface temperatures, increase the near-surface potential temperature deficit, and thereby strengthen the katabatic winds
341 over the upper portion of the steep margins of the ice sheet (Fig. 8b) (van den Broeke et al., 2009b; Gortler et al., 2014). Stronger
342 katabatic winds then increase turbulent heat flux by mixing relatively warm air through the stable boundary layer to the surface
343 (Fig. 7g, h).
344

345 While the differences in the radiative terms considerably outweigh those of the turbulent fluxes in $PGW_{SSC}^{T,Q}$, this is not the case
346 for PGW_{SSC} . Although the minor differences in SWD and LWD are more widespread (Fig. 7e, f), the impact of SSCs on

347 turbulent heat flux is greater in some locations along the ice sheet margins, particularly as is evident in the reduction in SHF
 348 along the northern and central portions of the western ablation zone (Fig. 7g). This appears to be primarily a consequence of
 349 the indirect katabatic wind adjustment. The lower SST and higher SIC in PGW_{SSC} reduces the horizontal temperature gradient
 350 between the ice sheet and surrounding seas which, as has been documented in previous work (Noël et al., 2014), causes a
 351 weakening of the katabatic wind along the ice sheet margins (Fig. 8c)—a change that would reduce turbulent mixing, and thus
 352 SHF, to the surface, while also causing a reduction in evaporation / sublimation and increasing LHF relative to the control.



353 **Figure 8: Melt season katabatic wind field under contrasting thermodynamic background conditions.** (a) 2000–2019 long-term mean
 354 Jun–Aug 10 m wind speed (shading) and direction (vectors). (b) Difference in 10 m wind speed between $PGW_{SSC}^{T,Q}$ and the control. (c)
 355 Difference in the 10 m wind speed between PGW_{SSC} and the control. $\Delta = PGW - \text{Control}$. Contour interval: 500 m. Range: 1000–3000 m.
 356
 357

358 The consistent and widespread reduction in LWD in $PGW_{SSC}^{T,Q}$ (Fig. 7b and f) is not surprising given the drier atmospheric
 359 conditions that prevailed during the preindustrial period. The spatial distribution of integrated water vapor (IWV) anomalies
 360 with respect to the control closely resemble that for LWD (c.f. Fig. 9e and 7f). Note that the LWD anomalies in Fig. 7b and f
 361 do not provide a complete picture of the impact on the SEB, as any resulting change in the temperature of the ice sheet's
 362 surface would be offset to some degree by a change in emitted longwave radiation in accordance with the Planck feedback.
 363 This can be seen in Fig. S5, which depicts a weaker and less uniform response across the ice sheet when considering the

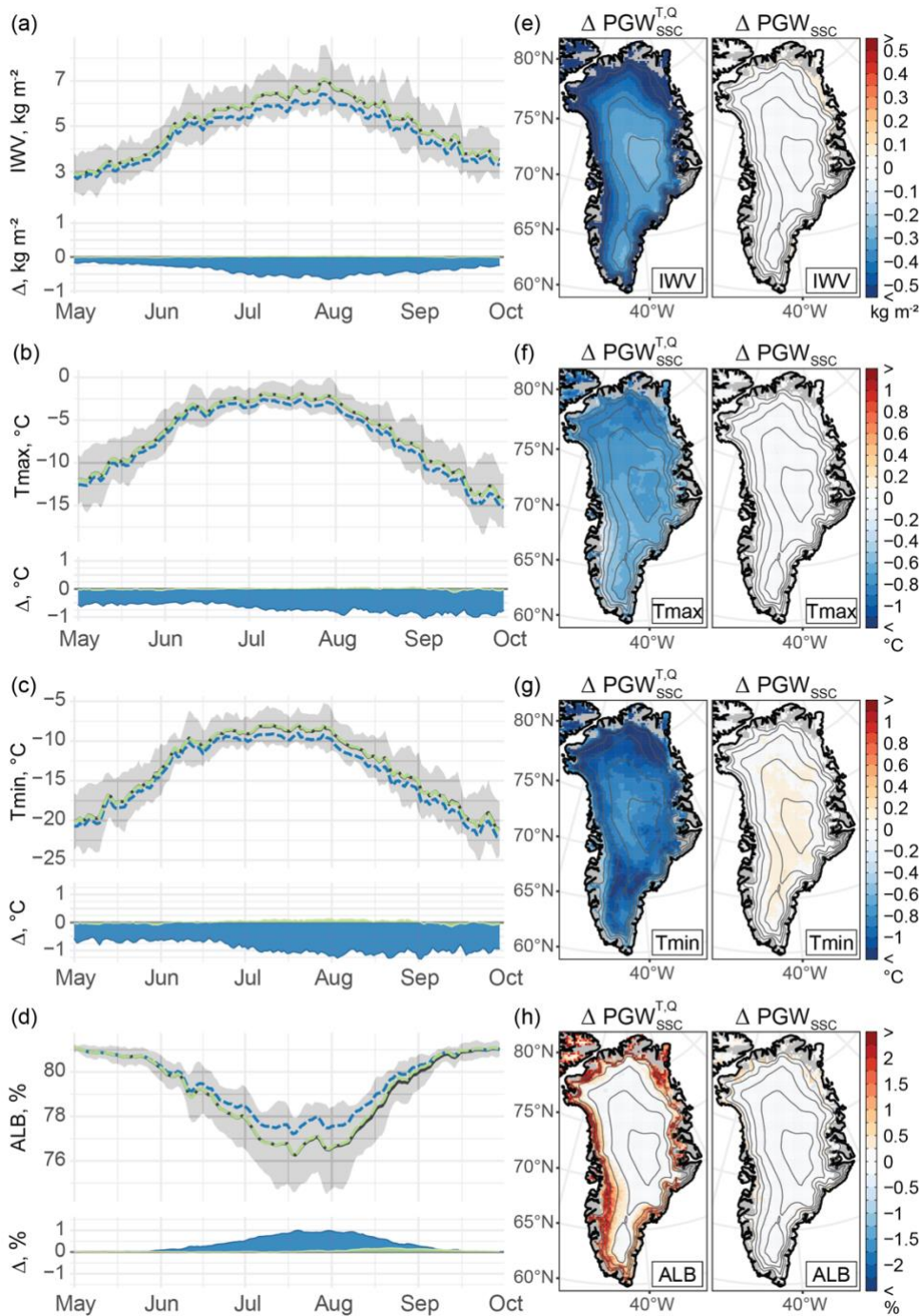
364 difference in net longwave radiation between $PGW_{SSC}^{T,Q}$ and the control; however, it remains the case that the preindustrial
365 setting of $PGW_{SSC}^{T,Q}$ produces reductions in net longwave radiation that are most evident over northern Greenland.

366

367 The consequence of this water vapor feedback can be seen in the ice-sheet-wide drop in surface temperature in $PGW_{SSC}^{T,Q}$. The
368 difference between the daily maximum (Tmax) and minimum (Tmin) temperature between $PGW_{SSC}^{T,Q}$ and the control both
369 increase from spring into fall (Fig. 9b, c). This seasonal pattern is consistent with stronger Arctic amplification in the fall than
370 in spring as pan-Arctic reductions in SIC in a warmer climate allow for increased heat flux from the ocean to the comparatively
371 cool fall atmosphere (Chung et al., 2021). Additionally, there is a decline in downward shortwave radiation as the solar
372 declination decreases into winter, which elevates the relative contribution of longwave radiative effects to the SEB (Lenaerts
373 et al., 2019; Wang et al., 2018, 2019). There is a distinct north-south gradient in the Tmax response (Fig. 9f). The weaker
374 Tmax differences over southern Greenland in $PGW_{SSC}^{T,Q}$ are a consequence of both a higher sun angle at lower latitudes and the
375 lower surface albedo of the southern ice sheet, both of which decrease the relative longwave contribution to the SEB. At night,
376 LWD constitutes the sole radiative input to the SEB. Consequently, the Tmin response is notably greater than Tmax and it
377 more closely resembles that of IWV (Fig. 9e) and LWD (Fig. 7f).

378

379 $PGW_{SSC}^{T,Q}$ exhibits a band of higher surface albedo throughout the melt season that runs along the perimeter of the ice sheet (Fig.
380 9d, h) and closely aligns with areas where IWV (Fig. 9e), Tmin, (Fig. 9g), SHF (Fig. 7g), and surface runoff (Fig. S3a) are
381 reduced relative to the control. Thus, the longwave radiative response to reduced water vapor content combined with
382 diminished SHF in a cooler atmosphere appear to be critical factors contributing to lower surface runoff under the preindustrial
383 background conditions of $PGW_{SSC}^{T,Q}$. The reduction in water vapor decreases LWD, which allows for lower Tmin. These changes
384 would reduce runoff by increasing the portion of meltwater that is refrozen within the snowpack and by diminishing the ice-
385 albedo feedback. The interdependence between SEB components is effectively illustrated by the differences in net shortwave
386 radiation between $PGW_{SSC}^{T,Q}$ and the control (Fig. S5)—the magnitude of the differences in net shortwave radiation exceeds that
387 for SWD along the perimeter of the ice sheet, emphasizing the importance of the ice albedo feedback. That the strongest signal
388 is located over the northern Greenland and aligned with some of the largest increases in surface albedo supports previous work
389 demonstrating the importance of this longwave radiative mechanism to runoff from northern Greenland (Noël et al., 2014).



390

391 **Figure 9. Thermodynamic mechanisms of SMB change.** (a–d) Top portion of each panel shows the 2000–2019 long-term daily mean
 392 values of each variable throughout the melt season for the control (gray), $PGW_{SSC}^{T,Q}$ (blue dashed), and PGW_{SSC} (green dashed) simulations.
 393 Gray shading shows the 1σ range about the mean for the control simulation. Time series represent the spatial average taken over the entire

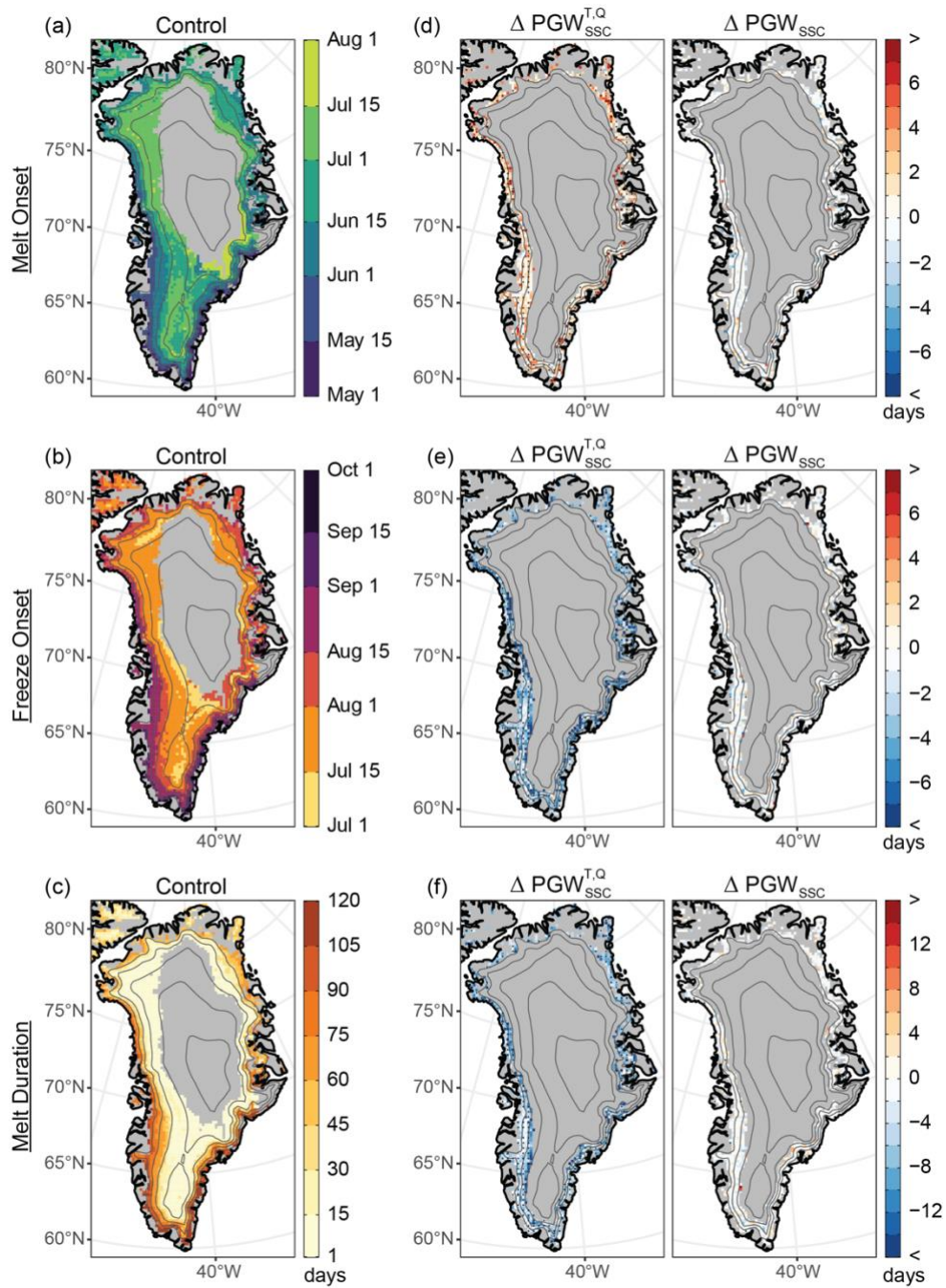
394 ice mask for a given variable. Bottom portion shows the difference between each PGW simulation ($PGW_{SSC}^{T,Q}$, blue; PGW_{SSC} , green) and
395 the control ($\Delta = PGW - \text{Control}$). (e–f) Maps depicting the difference between the 2000–2019, Jun–Aug long-term mean of each variable
396 between the PGW simulations ($PGW_{SSC}^{T,Q}$, left; PGW_{SSC} , right) and the control. Variables are organized by row: (a, e) integrated water vapor
397 (IWV); (b, f) daily maximum surface air temperature (Tmax); (c, g) daily minimum surface air temperature (Tmin); (d, h) surface albedo
398 (ALB). Contour interval: 500 m. Range: 1000–3000 m.
399

400 Focusing on PGW_{SSC} , there is no clear pattern of influence on IWV or near surface air temperature (Fig. 9e–g), and an
401 examination of temperature and humidity at 600 hPa shows no evidence of any appreciable influence on these variables in the
402 free atmosphere (Fig. S4). There is, however, an increase in surface albedo along the western and northern margins of the ice
403 sheet in PGW_{SSC} relative to the control that occurs late in the melt season (Fig. 9d, h) and appears to be the product of the
404 collocated reduction in SHF (Fig. 7g).

405 3.3. Thermodynamic Change and Melt Timing

406 Consistent with previous studies (Hanna et al., 2009, 2014; Noël et al., 2014), the above results suggest that direct local marine
407 influence on melt is limited to the outermost margins of the ice sheet. Furthermore, these results demonstrate that the influence
408 of local sea-surface conditions is an order of magnitude less than what is observed for the full thermodynamic forcing of
409 $PGW_{SSC}^{T,Q}$ (Fig. 4). To examine whether local SSC change may impact melt timing, Fig. 10 presents the results of a paired,
410 signed-rank test comparing differences in median melt and freeze onset between the control and each of the PGW simulations.
411 At lower elevations, melt onset during the 2000–2019 study period typically occurs between early-May and mid-June (Fig.
412 10a) while freeze onset occurs from early-August through September (Fig. 10b). Later melt onset and earlier freeze onset is
413 evident over higher elevations; however, melt in these regions is typically short-lived (Fig. 10c) and infrequent. Accordingly,
414 the comparisons of melt timing are limited to lower elevation locations with a sufficient sample of years with melt.

415
416 Relative to the control, the median date of melt onset in $PGW_{SSC}^{T,Q}$ occurs, on average, ~ 2.5 days later, while grid cells with
417 differences in the upper quartile showed delays in median melt onset of ≥ 4 days (Fig. 10d). Meanwhile, the median date of
418 freeze onset advanced, by ~ 3.7 days on average and freeze onset in the upper quartile of grid cells shifted to ≥ 5.5 days earlier
419 (Fig. 10e). Combined, these changes shortened the median melt season duration by an average of ~ 6.7 days, while melt duration
420 in the upper quartile of grid cells shortened by ≥ 9 days. For all melt timing metrics, the differences between the $PGW_{SSC}^{T,Q}$ and
421 the control that were deemed statistically significant at the 95% confidence level are widespread (Fig. 10d–f). In contrast,
422 differences between PGW_{SSC} and the control exhibit a weak and inconsistent signal for all melt timing metrics and yielded
423 only sporadic instances of statistically significant results.



424
425
426
427
428

Figure 10. The impact of thermodynamic change on melt timing. The observed median date of (a) melt onset, (b) freeze onset and (c) median melt season duration for the control simulation alongside (d–f) the difference between the PGW simulations ($PGW_{SSC}^{T,Q}$, left; PGW_{SSC} , right) and the control ($\Delta = PGW - \text{Control}$) for each metric as organized by row and labeled on the left. Stippling indicates differences that are statistically significant at the 95% confidence level. Contour interval: 500 m. Range: 1000–3000 m.

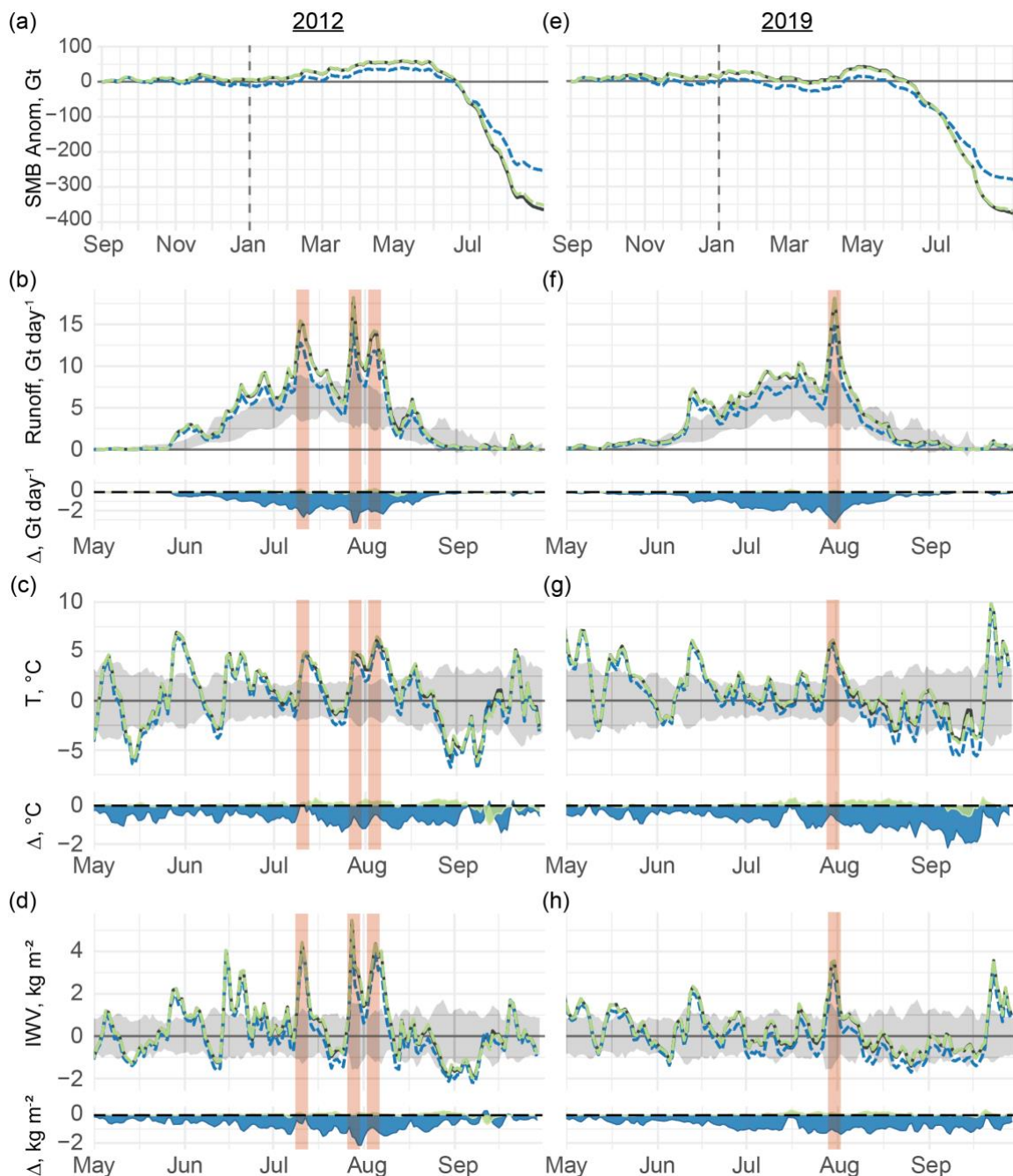
429 3.4. The Exceptional Melt Years of 2012 and 2019

430 Embedded in the long-term SMB decline (Fig. 4), 2012 and 2019 stand out as exceptional years of surface mass loss. According
431 to the control simulation, there was a cumulative SMB anomaly of -364 Gt during the 2011–2012 hydrological year (Fig. 11a).
432 The melt season of 2012 was characterized by recurrent episodes of intense surface runoff (Fig. 11b). Pronounced atmospheric
433 ridging over Greenland promoted southerly advection of warm, moist air to the western ice sheet (Hermann et al., 2020; Neff
434 et al., 2014), generating strong turbulent heat fluxes that drove high-volume meltwater production over the western ablation
435 zone (Cullather et al., 2020; Fausto et al., 2016b). Adiabatic cooling of remotely-sourced moist air that ascended the western
436 slope of the ice sheet on July 12 prompted the formation of low-level, liquid clouds that supplied the requisite longwave
437 radiative forcing for widespread melt over high elevations (Bennartz et al., 2013; Neff et al., 2014), generating a single day
438 melt extent that covered over 98% of the ice sheet's surface (Nghiem et al., 2012).

439
440 The cumulative SMB anomaly over the 2018–2019 hydrological year totaled -376 Gt (Fig. 11e). The melt season of 2019 was
441 heavily influenced by a blocking anticyclone, with origins in the European heatwave of the same year (Cullather et al., 2020;
442 Hanna et al., 2021), that produced tremendous surface runoff during a melt event centered around July 31 (Fig. 11f). The air
443 mass, which was transported west from Europe, was warmer and drier in comparison with that which was responsible for the
444 mid-July, 2012 melt event and, consequently, did not produce the same low-level cloud cover that was instrumental to melt of
445 the accumulation zone in 2012 (Tedesco and Fettweis, 2020). Consequently, while the total surface mass loss in 2019 was
446 comparable to that of 2012, observed melt was not as extensive in 2019, reaching a maximum coverage of ~73% of the ice
447 sheet's surface on July 31 (Tedesco and Fettweis, 2020).

448
449 For both years, the portion of observed surface mass loss that is attributable to changes in the local background thermodynamic
450 environment was less than the average for the study period: whereas the anomalous mass loss over the entire 2000–2019 study
451 period was ~62% less in $PGW_{SSC}^{T,Q}$ relative to the control, the reduction in mass loss was a relatively modest 30% and 25% in
452 2012 and 2019, respectively (Fig. 11a, e). This suggests that the record melt observed during those two summers is more a
453 consequence of exceptional atmospheric circulation patterns than it is a direct consequence of the long-term warming trend;
454 however, these exceptional circulation patterns and the long-term temperature trend may not be independent, as some studies
455 have suggested more persistent circulation regimes under global warming (Coumou et al., 2018; Overland et al., 2012; Preece
456 et al., 2023b; Screen, 2013). This disparity is also evident over synoptic timescales—the periods of strong dynamical forcing,
457 marked by the red, vertical bars in Fig. 11, correspond to local minima in the differences in daily-mean near-surface air
458 temperature between $PGW_{SSC}^{T,Q}$ and the control. The production of meltwater and consequent surface runoff during high-volume
459 melt events is largely driven by turbulent heat fluxes (Box et al., 2022; Fausto et al., 2016b, a). It follows that the longwave
460 radiative effects of the water vapor feedback that are dictated by changes in the thermodynamic environment assume a lesser
461 role during these periods of intense melt. The minimal difference between PGW_{SSC} and the control suggests no appreciable

462 direct thermodynamic contribution by the observed change in local SSCs to runoff production during these exceptional melt
463 years.



464 **Figure 11. Thermodynamic contribution to surface mass loss during years of exceptional melt.** Panels show (a, e) the cumulative SMB
465 anomaly spanning the Sep–Aug hydrological year alongside (b, f) total daily meltwater runoff, (c, g) mean daily near-surface air temperature
466 anomaly, and (d, h) mean daily integrated water vapor anomaly during the exceptional melt years of (a–d) 2012 and (e–h) 2019. In all panels,

467 time series are presented for the control (gray), $PGW_{SSC}^{T,Q}$ (blue dashed), and PGW_{SSC} (green dashed) simulations. Bottom portion of b–d
468 and f–h shows the difference between each PGW simulation ($PGW_{SSC}^{T,Q}$, blue; PGW_{SSC} , green) and the control ($\Delta = PGW - \text{Control}$). Red
469 vertical shading highlights periods of strong synoptic-scale forcing. Cumulative anomalies in (a, e) calculated with respect to the 1980–1989
470 reference period. Anomalies in (b–d, f–h) calculated with respect to the entire 2000–2019 study period and represent the spatial average taken
471 over the entire ice mask for a given variable.
472

473 Meltwater runoff is primarily sourced from the ablation zone and is therefore controlled by processes, such as turbulent heat
474 flux and downward solar radiation (due to the low albedo), that exert a strong influence along the margins. Melt in the
475 accumulation zone (with high albedo) is more dependent on longwave radiative effects and presence of clouds. Given the
476 consistent reduction in water vapor content in $PGW_{SSC}^{T,Q}$ relative to the control (Fig. 11d,h), the influence of thermodynamic
477 change during these years of extreme mass loss may be more visible in the frequency of melt over the accumulation zone than
478 for total meltwater runoff.
479

480 In the control, melt frequencies across the ice sheet were generally greater in 2012 than 2019 (Fig. S6a, c). This is evident over
481 the southern portion of the ice sheet, where locations above 2500 m in elevation recorded over 40 days of melt in 2012 (Fig.
482 S6a). Melt was also more frequent above ~1500 m over the northern ice sheet in 2012, but 2019 underwent more frequent melt
483 at lower elevations of the most northern margin of the ice sheet due, in part, to early melt onset and below-normal snow
484 accumulation which augmented melt through the melt-albedo feedback (Bailey and Hubbard, 2025; Tedesco and Fettweis,
485 2020). The difference between $PGW_{SSC}^{T,Q}$ and the control shows that the thermodynamic contribution to melt frequency was
486 greater in 2019 than 2012 (Fig. S6b, d). Unlike 2019, intense water vapor transport accompanied the extensive melt events of
487 2012 (Hermann et al., 2020; Neff et al., 2014; Tedesco and Fettweis, 2020). Thus, the longwave radiative forcing necessary
488 for melt over the accumulation zone was supplied by the large-scale circulation, which likely resulted in less sensitivity to
489 changes in local thermodynamic conditions. While the reduction in melt frequency of 1 to 5 days at elevations above ~2000
490 m in northern and central Greenland is low compared to other regions of the ice sheet, it is comparable to the total observed
491 number of melt days in the control (c.f. Fig. S6a, c and b, d), demonstrating that melt over much of the high accumulation zone
492 would not have occurred if not for recent climate warming. The changes in the number of PGW_{SSC} melt days relative to the
493 control are minimal and generally do not exhibit a coherent spatial signal (Fig. S6b, d); however, there is some indication of a
494 decline in 2019 melt frequency over the southwestern ice sheet that is opposed by an increase in melt frequency above 2000
495 m (Fig. S6d).

496 **4. Discussion and Conclusions**

497 Much of the work examining the recent increase in Greenland Ice Sheet meltwater runoff has rightfully focused on the role of
498 atmospheric dynamics (Bevis et al., 2019; Fettweis et al., 2013; Hanna et al., 2015, 2016, 2018b, 2022; Hofer et al., 2017).
499 While some have presented evidence of a relationship between global climate change and the shift in summer atmospheric

500 circulation that has promoted melt of the ice sheet (Liu et al., 2016; Preece et al., 2023b; Screen, 2013), a conclusive link
501 remains a subject of investigation. In contrast, the accelerated rate of warming in the Arctic represents a robust climate change
502 signal that has undoubtedly contributed to recent SMB trends (Boers and Rypdal, 2021; Hanna et al., 2008). This work
503 represents, to our knowledge, the first systematic attempt to quantify the contribution of the local change in background
504 thermodynamic conditions to recent surface mass loss.

505
506 Our results indicate that had the large-scale atmospheric circulation that was observed from 2000–2019 occurred under
507 preindustrial thermodynamic background conditions, the cumulative SMB anomaly would have been reduced by over 62%
508 (Fig. 4). The mechanisms by which local thermodynamic background conditions contribute to SMB change appear to be
509 dominated by longwave radiative effects stemming from the water vapor feedback. The amplified rate of warming in the Arctic
510 has augmented surface runoff by promoting an increase in atmospheric moisture and associated downward longwave radiation
511 (Fig. 9a, e and 7b, f), which disproportionately increases daily minimum temperatures (Fig. 9c, g). These results are consistent
512 with Orsi et al. (2017), which identifies a positive trend in 1982–2011 surface air temperature reconstructed from borehole
513 temperature measurements at the North Greenland Eemian Ice Drilling site in northwest Greenland. They point to an increase
514 in downward longwave flux and associated feedbacks as the primary contributor to the warming trend. Likewise, Noël *et al.*
515 (2019) show that an increase in downward longwave radiation has caused a disproportionate increase in surface runoff from
516 the northern drainages by promoting melt and expanding the ablation zone in this region of high albedo, and by increasing
517 daily minimum temperatures, which reduces meltwater refreeze within the firn layer. While the authors point to the advection
518 of moisture-rich air to the northern ice sheet by anomalously anticyclonic summer circulation over Greenland, the results of
519 this analysis suggest that the increase in background temperature constitutes an important contribution to this mechanism on
520 its own.

521
522 The ~62% reduction, which is conditional on the ERA5 2000–2019 circulation occurring under preindustrial thermodynamic
523 conditions, does not imply that atmospheric circulation is only responsible for 38% of the observed impact on SMB, as the
524 individual contributions of atmospheric dynamics and thermodynamics should sum to the *total* change in SMB relative to what
525 it would have been if neither an increased frequency of Greenland blocking nor anthropogenic warming had occurred. Given
526 that the ice sheet maintained a positive cumulative SMB anomaly through 2009 under the preindustrial thermodynamic
527 background conditions imposed in $PGW_{SSC}^{T,Q}$, it is possible that the cumulative anomaly may have remained positive through
528 the end of the study period if not for the increased frequency of anomalous anticyclones. Thus, relative to this hypothetical
529 preindustrial climate with more typical atmospheric circulation, the total change in SMB would be greater than the magnitude
530 of the negative anomalies presented in Fig. 4 and the contribution of atmospheric circulation to this total change would exceed
531 38%. Indeed, using an earth system model to nudge the wind field toward observed conditions while maintaining constant
532 external forcing, Topál et al. (2022) showed that changes in atmospheric circulation explained 56% of the increase in surface
533 air temperature over Greenland from 1990 to 2012. Using historical data and a circulation analogue technique, Fettweis et al.

534 (2013) found that the shift in summer circulation explained ~70% of the 1993–2012 warming at 700 hPa over Greenland.
535 Focusing on mass loss, Delhasse et al. (2018) compared output from MAR forced by perturbed reanalysis data from the recent
536 period of increased Greenland blocking against simulations forced by output from GCMs which have collectively failed to
537 capture this change in circulation (Delhasse et al., 2021; Hanna et al., 2018a). Their results suggest that if the recent anomalous
538 circulation persists into the future, the ice sheet will undergo more than twice the surface mass loss that is currently projected
539 by GCMs. Thus, understanding this circulation change and why it is not represented in climate models must be a top priority
540 for accurate projections of Greenland Ice Sheet mass loss.

541
542 The contribution of local thermodynamic background conditions to total surface mass loss during the exceptional melt years
543 of 2012 and 2019 was less than half that which was observed for the entire 2000–2019 study period (c.f. Fig. 4 and 11a, e),
544 suggesting that the relative thermodynamic contribution is reduced during strong large-scale atmospheric forcing. This is also
545 evident over synoptic timescales, where the difference in surface air temperature between $PGW_{SSC}^{T,Q}$ and the control is minimized
546 on days of exceptional surface runoff; rather, the greatest differences in surface temperature emerge during periods
547 encompassing temporal minima in air temperature (Fig. 11). This likely reflects the increased contribution of remotely sourced
548 heat and moisture during periods of strong large-scale forcing, which would reduce the relative importance of the longwave
549 radiative effects that typify the response to changes in the thermodynamic background state. In other words, recent local
550 thermodynamic change around Greenland appears to have promoted surface runoff by raising the floor of the temperature
551 distribution more so than by exacerbating warm extremes. This signal may be due in part to biases inherent to the PGW
552 approach. The application of a monthly mean climate perturbation may underrepresent the true change in air temperature and
553 water vapor concentration during extreme events such as the blocking episodes and attendant atmospheric rivers that have
554 promoted melt of the ice sheet. While the thermodynamic fields are free to adjust in accordance with any relevant nonlinear
555 processes within the MAR integration domain, it is likely that any biases at the model boundaries would be conveyed to the
556 ice sheet to some extent. Despite these shortcomings, the PGW method of downscaling is recognized as an effective means of
557 isolating the thermodynamic component of climate change (Gutmann et al., 2018; Lackmann, 2015; Mallard et al., 2013;
558 Rasmussen et al., 2020)– an approach that has been advocated particularly in cases of extreme events for which the governing
559 dynamics are not well represented in the models (Lloyd and Oreskes, 2018; Trenberth et al., 2015), which is true of both
560 atmospheric rivers and atmospheric blocking (Delhasse et al., 2021; Hanna et al., 2018a; Wang et al., 2023; Woollings et al.,
561 2018).

562
563 The same large-scale atmospheric conditions that typify our control period and have encouraged mass loss have also fostered
564 below-normal sea ice in the region (Ballinger et al., 2018; Ogi and Wallace, 2007; Stroeve et al., 2017). Thus, the 1880–1899
565 sea ice climatology that we prescribe here may often exceed the SIC that would have occurred if the recently observed
566 atmospheric circulation had occurred under preindustrial conditions. Recognizing this potential bias, our results likely
567 represent an aggressive estimate of the contribution of SSCs to recent surface mass loss. Even so, this analysis reveals minimal

568 direct thermodynamic contribution by local SSCs, supporting previous work showing low SMB sensitivity to adjacent SSCs
569 due to the barrier to onshore advection from the marine layer presented by consistent katabatic outflow over the ice sheet
570 (Hanna et al., 2009, 2014; Noël et al., 2014).

571
572 Regarding the hypothesis of Stroeve *et al.* (2017) that declining SIC may promote earlier melt onset, thereby preconditioning
573 the ice sheet for greater meltwater production later in the season, our results suggest limited direct thermodynamic impact of
574 local SSCs on recent surface melt and no discernable impact on melt timing (Fig. 4 and 10). There are several plausible reasons
575 for this apparent disparity. First, our interpretation assumes that SSCs and ocean-atmosphere coupling are accurately
576 represented by the model. Gridded climate datasets, with their relatively coarse spatial resolution, are less accurate in areas
577 that rely more heavily on spatial interpolation, such as along coastlines and near the sea ice front where in-situ observations
578 are less frequent (Hanna et al., 2006; Hurrell et al., 2008; Yang et al., 2021). This could degrade model representation of ocean-
579 atmosphere coupling; however, the disparities among various gridded SST and SIC datasets are generally much smaller than
580 the long-term trends (Yang et al., 2021) and, therefore, should exert minimal influence on the signal that we seek to quantify.
581 Second, our experimental design did not examine the isolated contribution of changes in the atmospheric fields alone, and it
582 is possible that nonlinear interactions between changes in SSCs and atmospheric thermodynamic fields caused the combined
583 influence in $PGW_{SSC}^{T,Q}$ to be greater than the sum of their individual contributions. Lastly, our analysis did not examine any
584 indirect effects via alteration of the large-scale circulation by changes in SSCs. Both model- and observation-based studies
585 have yielded evidence of a link between declining sea ice in Baffin Bay and the observed increase in summer Greenland
586 blocking (Liu et al., 2016; Screen, 2013; Sellevold et al., 2022; Wu et al., 2013). Indeed, Stroeve et al. (2017) found that the
587 statistical relationship between ice sheet melt and Baffin Bay SIC weakened considerably and, consistent with the PGW_{SSC}
588 response in Fig. 5c, became more confined to the periphery of the western ice sheet after correcting for the influence of
589 Greenland blocking. Considered in conjunction with our results, this suggests that this indirect pathway of influence could
590 help explain the statistical relationship between SSCs and early melt onset.

591
592 Because MAR assumes a fixed ice sheet geometry, the results presented herein strictly describe the thermodynamic influence
593 on the SMB of the ice sheet; however, surface runoff and solid ice dynamics are not independent. Strong pulses of meltwater
594 can cause rapid drainage through moulins that overwhelms the subglacial drainage network (Chu, 2014; Schoof, 2010), causing
595 a surge in ice velocity that increases glacial discharge and accelerates ice sheet thinning (Andersen et al., 2011; Chu, 2014;
596 Schoof, 2010). Thus, it is likely that the thermodynamic influence on surface melt documented here has indirectly contributed
597 further to sea-level rise via its impact on ice sheet dynamics. Regardless, these results demonstrate that while the shift in
598 summer atmospheric circulation over Greenland has been key to the acceleration of runoff from the ice sheet, the change in
599 the background thermodynamic state under Arctic amplification has markedly enhanced the observed surface mass loss beyond
600 that which would have occurred if not for anthropogenic climate change.

601 **Code and Data Availability**

602 MAR data from this study are available through the Arctic Data Center at <https://doi.org/10.18739/A2TT4FV6W> (Preece et
603 al., 2023a). ERA5 reanalysis data used to force the model can be accessed through the Copernicus Climate Data Store at
604 <https://doi.org/10.24381/CDS.BD0915C6> (Copernicus Climate Change Service, 2018). CESM-LE data used adjust the
605 boundary conditions are available through the National Science Foundation (NSF) National Center for Atmospheric Research
606 (NCAR) Research Data Archive at <https://doi.org/10.5065/D6J101D1> (Kay et al., 2021). Merged Hadley-OI SIC and SST
607 fields are hosted through Zenodo at <https://doi.org/10.5065/R33V-SV91> (Hurrell et al., 2020).

608 **Author Contribution**

609 JP, TM, and PA conceptualized the study. JP, PA, and GK designed the model experiments. JP, PA, and XF performed the
610 model simulations. TM and MT led the project administration and funding acquisition. MT and PA supplied the computing
611 resources. JP performed the formal analysis and prepared the manuscript in consultation with all co-authors.

612 **Competing Interests**

613 At least one of the (co-)authors is a member of the editorial board of The Cryosphere.

614 **Acknowledgements**

615 Computing resources to perform the MAR simulations were provided by the Lamont-Doherty Earth Observatory.

616 **Financial Support**

617 This work was supported by NSF Arctic Systems Science award number 1900324, Strategic Environmental Research and
618 Development Program project number RC18-1658, NASA award 80NSSC17K0351 and Heising Simons Foundation award #
619 HSFOUNF 2019 - 1160. G.J.K. acknowledges support from the U.S. Department of Energy (DOE) Regional and Global Model
620 Analysis (RGMA) Program (DE-SC0021209).

621 **References**

622 Amory, C., Kittel, C., Le Toumelin, L., Agosta, C., Delhasse, A., Favier, V., and Fettweis, X.: Performance of MAR (v3.11)
623 in simulating the drifting-snow climate and surface mass balance of Adélie Land, East Antarctica, *Geoscientific Model*
624 *Development*, 14, 3487–3510, <https://doi.org/10.5194/gmd-14-3487-2021>, 2021.

- 625 Andersen, M. L., Nettles, M., Elosegui, P., Larsen, T. B., Hamilton, G. S., and Stearns, L. A.: Quantitative estimates of velocity
626 sensitivity to surface melt variations at a large Greenland outlet glacier, *Journal of Glaciology*, 57, 609–620,
627 <https://doi.org/10.3189/002214311797409785>, 2011.
- 628 Bailey, H. and Hubbard, A.: Snow Mass Recharge of the Greenland Ice Sheet Fueled by Intense Atmospheric River,
629 *Geophysical Research Letters*, 52, e2024GL110121, <https://doi.org/10.1029/2024GL110121>, 2025.
- 630 Ballinger, T. J., Hanna, E., Hall, R. J., Miller, J., Ribergaard, M. H., and Høyer, J. L.: Greenland coastal air temperatures linked
631 to Baffin Bay and Greenland Sea ice conditions during autumn through regional blocking patterns, *Clim Dyn*, 50, 83–100,
632 <https://doi.org/10.1007/s00382-017-3583-3>, 2018.
- 633 Ballinger, T. J., Mote, T. L., Mattingly, K., Bliss, A. C., Hanna, E., van As, D., Prieto, M., Gharehchahi, S., Fettweis, X., Noël,
634 B., Smeets, P. C. J. P., Ribergaard, M. H., and Cappelen, J.: Greenland Ice Sheet late-season melt: Investigating multi-scale
635 drivers of K-transect events, *The Cryosphere Discuss.*, 1–23, <https://doi.org/10.5194/tc-2018-285>, 2019.
- 636 Bennartz, R., Shupe, M. D., Turner, D. D., Walden, V. P., Steffen, K., Cox, C. J., Kulie, M. S., Miller, N. B., and Pettersen,
637 C.: July 2012 Greenland melt extent enhanced by low-level liquid clouds, *Nature*, 496, 83–86,
638 <https://doi.org/10.1038/nature12002>, 2013.
- 639 Bevis, M., Harig, C., Khan, S. A., Brown, A., Simons, F. J., Willis, M., Fettweis, X., Broeke, M. R. van den, Madsen, F. B.,
640 Kendrick, E., Caccamise, D. J., Dam, T. van, Knudsen, P., and Nylen, T.: Accelerating changes in ice mass within Greenland,
641 and the ice sheet’s sensitivity to atmospheric forcing, *PNAS*, 116, 1934–1939, <https://doi.org/10.1073/pnas.1806562116>, 2019.
- 642 Boers, N. and Rypdal, M.: Critical slowing down suggests that the western Greenland Ice Sheet is close to a tipping point,
643 *Proceedings of the National Academy of Sciences*, 118, e2024192118, <https://doi.org/10.1073/pnas.2024192118>, 2021.
- 644 Bonsoms, J., González-Herrero, S., Fettweis, X., Lemus-Cánovas, M., Oliva, M., and López-Moreno, J. I.: Record-breaking
645 Greenland ice sheet melt events under recent and future climate, *Nat Commun*, 17, 3605, <https://doi.org/10.1038/s41467-026-69543-5>, 2026.
- 647 Box, J. E., Cressie, N., Bromwich, D. H., Jung, J.-H., Van Den Broeke, M., Van Angelen, J. H., Forster, R. R., Miège, C.,
648 Mosley-Thompson, E., Vinther, B., and McConnell, J. R.: Greenland Ice Sheet Mass Balance Reconstruction. Part I: Net Snow
649 Accumulation (1600–2009), *Journal of Climate*, 26, 3919–3934, <https://doi.org/10.1175/JCLI-D-12-00373.1>, 2013.
- 650 Box, J. E., Wehrlé, A., van As, D., Fausto, R. S., Kjeldsen, K. K., Dachauer, A., Ahlstrøm, A. P., and Picard, G.: Greenland
651 Ice Sheet Rainfall, Heat and Albedo Feedback Impacts From the Mid-August 2021 Atmospheric River, *Geophysical Research
652 Letters*, 49, e2021GL097356, <https://doi.org/10.1029/2021GL097356>, 2022.
- 653 Box, J. E., Nielsen, K. P., Yang, X., Niwano, M., Wehrlé, A., van As, D., Fettweis, X., Køltzow, M. A. Ø., Palmason, B.,
654 Fausto, R. S., van den Broeke, M. R., Huai, B., Ahlstrøm, A. P., Langley, K., Dachauer, A., and Noël, B.: Greenland ice sheet
655 rainfall climatology, extremes and atmospheric river rapids, *Meteorological Applications*, 30, e2134,
656 <https://doi.org/10.1002/met.2134>, 2023.
- 657 van den Broeke, M. R., Bamber, J., Ettema, J., Rignot, E., Schrama, E., Berg, W. J. van de, Meijgaard, E. van, Velicogna, I.,
658 and Wouters, B.: Partitioning Recent Greenland Mass Loss, *Science*, 326, 984–986, <https://doi.org/10.1126/science.1178176>,
659 2009a.
- 660 van den Broeke, M. R., Smeets, P., and Ettema, J.: Surface layer climate and turbulent exchange in the ablation zone of the
661 west Greenland ice sheet, *International Journal of Climatology*, 29, 2309–2323, <https://doi.org/10.1002/joc.1815>, 2009b.

- 662 van den Broeke, M. R., Enderlin, E. M., Howat, I. M., Kuipers Munneke, P., Noël, B. P. Y., van de Berg, W. J., van Meijgaard,
663 E., and Wouters, B.: On the recent contribution of the Greenland ice sheet to sea level change, *The Cryosphere*, 10, 1933–
664 1946, <https://doi.org/10.5194/tc-10-1933-2016>, 2016.
- 665 Bromwich, D. H., Cullather, R. I., Chen, Q., and Csathó, B. M.: Evaluation of recent precipitation studies for Greenland Ice
666 Sheet, *Journal of Geophysical Research: Atmospheres*, 103, 26007–26024, <https://doi.org/10.1029/98JD02278>, 1998.
- 667 Brun, E., Martin, E., Simon, V., Gendre, C., and Coléou, C.: An Energy and Mass Model of Snow Cover Suitable for
668 Operational Avalanche Forecasting, *J. Glaciol.*, 35, 333, <https://doi.org/10.1017/S0022143000009254>, 1989.
- 669 Brun, E., David, P., Sudul, M., and Brunot, G.: A numerical model to simulate snow-cover stratigraphy for operational
670 avalanche forecasting, *Journal of Glaciology*, 38, 13–22, <https://doi.org/10.3189/S0022143000009552>, 1992.
- 671 Caesar, L., Rahmstorf, S., Robinson, A., Feulner, G., and Saba, V.: Observed fingerprint of a weakening Atlantic Ocean
672 overturning circulation, *Nature*, 556, 191–196, <https://doi.org/10.1038/s41586-018-0006-5>, 2018.
- 673 Cattiaux, J., Peings, Y., Saint-Martin, D., Trou-Kechout, N., and Vavrus, S. J.: Sinuosity of midlatitude atmospheric flow in a
674 warming world, *Geophysical Research Letters*, 43, 8259–8268, <https://doi.org/10.1002/2016GL070309>, 2016.
- 675 Cazenave, A., Palanisamy, H., and Ablain, M.: Contemporary sea level changes from satellite altimetry: What have we
676 learned? What are the new challenges?, *Advances in Space Research*, 62, 1639–1653,
677 <https://doi.org/10.1016/j.asr.2018.07.017>, 2018.
- 678 Chu, V. W.: Greenland ice sheet hydrology: A review, *Progress in Physical Geography: Earth and Environment*, 38, 19–54,
679 <https://doi.org/10.1177/0309133313507075>, 2014.
- 680 Chung, E., Ha, K., Timmermann, A., Stuecker, M. F., Bodai, T., and Lee, S.: Cold-Season Arctic Amplification Driven by
681 Arctic Ocean-Mediated Seasonal Energy Transfer, *Earth’s Future*, 9, <https://doi.org/10.1029/2020ef001898>, 2021.
- 682 Clausen, H. B., Gundestrup, N. S., Johnsen, S. J., Bindshadler, R., and Zwally, J.: Glaciological Investigations in the Crête
683 Area, Central Greenland: A Search for a new Deep-Drilling Site, *Annals of Glaciology*, 10, 10–15,
684 <https://doi.org/10.3189/S0260305500004080>, 1988.
- 685 Cohen, J., Screen, J. A., Furtado, J. C., Barlow, M., Whittleston, D., Coumou, D., Francis, J., Dethloff, K., Entekhabi, D.,
686 Overland, J., and Jones, J.: Recent Arctic amplification and extreme mid-latitude weather, *Nature Geoscience*, 7, 627–637,
687 <https://doi.org/10.1038/ngeo2234>, 2014.
- 688 Copernicus Climate Change Service: ERA5 hourly data on pressure levels from 1940 to present,
689 <https://doi.org/10.24381/CDS.BD0915C6>, 2018.
- 690 Coumou, D., Lehmann, J., and Beckmann, J.: The weakening summer circulation in the Northern Hemisphere mid-latitudes,
691 *Science*, 348, 324–327, <https://doi.org/10.1126/science.1261768>, 2015.
- 692 Coumou, D., Di Capua, G., Vavrus, S., Wang, L., and Wang, S.: The influence of Arctic amplification on mid-latitude summer
693 circulation, *Nat Commun*, 9, 2959, <https://doi.org/10.1038/s41467-018-05256-8>, 2018.
- 694 Cullather, R. I., Andrews, L. C., Croteau, M. J., Digirolamo, N. E., Hall, D. K., Lim, Y.-K., Loomis, B. D., Shuman, C. A.,
695 and Nowicki, S. M. J.: Anomalous Circulation in July 2019 Resulting in Mass Loss on the Greenland Ice Sheet, *Geophysical
696 Research Letters*, 47, e2020GL087263, <https://doi.org/10.1029/2020GL087263>, 2020.

- 697 Davini, P. and D'Andrea, F.: From CMIP3 to CMIP6: Northern Hemisphere Atmospheric Blocking Simulation in Present and
698 Future Climate, *Journal of Climate*, 33, 10021–10038, <https://doi.org/10.1175/JCLI-D-19-0862.1>, 2020.
- 699 Delhasse, A., Fettweis, X., Kittel, C., Amory, C., and Agosta, C.: Brief communication: Impact of the recent atmospheric
700 circulation change in summer on the future surface mass balance of the Greenland Ice Sheet, *The Cryosphere*, 12, 3409–3418,
701 <https://doi.org/10.5194/tc-12-3409-2018>, 2018.
- 702 Delhasse, A., Hanna, E., Kittel, C., and Fettweis, X.: Brief communication: CMIP6 does not suggest any atmospheric blocking
703 increase in summer over Greenland by 2100, *International Journal of Climatology*, 41, 2589–2596,
704 <https://doi.org/10.1002/joc.6977>, 2021.
- 705 Di Capua, G. and Coumou, D.: Changes in meandering of the Northern Hemisphere circulation, *Environ. Res. Lett.*, 11,
706 094028, <https://doi.org/10.1088/1748-9326/11/9/094028>, 2016.
- 707 Fausto, R. S., van As, D., Box, J. E., Colgan, W., and Langen, P. L.: Quantifying the Surface Energy Fluxes in South Greenland
708 during the 2012 High Melt Episodes Using In-situ Observations, *Front. Earth Sci.*, 4, <https://doi.org/10.3389/feart.2016.00082>,
709 2016a.
- 710 Fausto, R. S., van As, D., Box, J. E., Colgan, W., Langen, P. L., and Mottram, R. H.: The implication of nonradiative energy
711 fluxes dominating Greenland ice sheet exceptional ablation area surface melt in 2012, *Geophysical Research Letters*, 43, 2649–
712 2658, <https://doi.org/10.1002/2016GL067720>, 2016b.
- 713 Fettweis, X., Gallée, H., Lefebvre, F., and van Ypersele, J.-P.: Greenland surface mass balance simulated by a regional climate
714 model and comparison with satellite-derived data in 1990–1991, *Climate Dynamics*, 24, 623–640,
715 <https://doi.org/10.1007/s00382-005-0010-y>, 2005.
- 716 Fettweis, X., Hanna, E., Lang, C., Belleflamme, A., Erpicum, M., and Gallée, H.: Brief communication: “Important role of the
717 mid-tropospheric atmospheric circulation in the recent surface melt increase over the Greenland ice sheet,” *The Cryosphere*,
718 7, 241–248, <https://doi.org/10.5194/tc-7-241-2013>, 2013.
- 719 Fettweis, X., Box, J. E., Agosta, C., Amory, C., Kittel, C., Lang, C., van As, D., Machguth, H., and Gallée, H.: Reconstructions
720 of the 1900–2015 Greenland ice sheet surface mass balance using the regional climate MAR model, *The Cryosphere*, 11,
721 1015–1033, <https://doi.org/10.5194/tc-11-1015-2017>, 2017.
- 722 Fettweis, X., Hofer, S., Krebs-Kanzow, U., Amory, C., Aoki, T., Berends, C. J., Born, A., Box, J. E., Delhasse, A., Fujita, K.,
723 Gierz, P., Goelzer, H., Hanna, E., Hashimoto, A., Huybrechts, P., Kapsch, M.-L., King, M. D., Kittel, C., Lang, C., Langen,
724 P. L., Lenaerts, J. T. M., Liston, G. E., Lohmann, G., Mernild, S. H., Mikolajewicz, U., Modali, K., Mottram, R. H., Niwano,
725 M., Noël, B., Ryan, J. C., Smith, A., Streffing, J., Tedesco, M., van de Berg, W. J., van den Broeke, M., van de Wal, R. S. W.,
726 van Kampenhout, L., Wilton, D., Wouters, B., Ziemens, F., and Zolles, T.: GrSMBMIP: intercomparison of the modelled 1980–
727 2012 surface mass balance over the Greenland Ice Sheet, *The Cryosphere*, 14, 3935–3958, [https://doi.org/10.5194/tc-14-3935-](https://doi.org/10.5194/tc-14-3935-2020)
728 2020, 2020.
- 729 Francis, J. A. and Vavrus, S. J.: Evidence linking Arctic amplification to extreme weather in mid-latitudes: ARCTIC LINKS
730 TO MID-LATITUDE WEATHER, *Geophys. Res. Lett.*, 39, L06801, <https://doi.org/10.1029/2012GL051000>, 2012.
- 731 Gallagher, M. R., Shupe, M. D., and Miller, N. B.: Impact of Atmospheric Circulation on Temperature, Clouds, and Radiation
732 at Summit Station, Greenland, with Self-Organizing Maps, *J. Climate*, 31, 8895–8915, [https://doi.org/10.1175/JCLI-D-17-](https://doi.org/10.1175/JCLI-D-17-0893.1)
733 0893.1, 2018.

- 734 Glaude, Q., Noel, B., Olesen, M., Van Den Broeke, M., Van De Berg, W. J., Mottram, R., Hansen, N., Delhasse, A., Amory,
735 C., Kittel, C., Goelzer, H., and Fettweis, X.: A Factor Two Difference in 21st-Century Greenland Ice Sheet Surface Mass
736 Balance Projections From Three Regional Climate Models Under a Strong Warming Scenario (SSP5-8.5), *Geophysical*
737 *Research Letters*, 51, e2024GL111902, <https://doi.org/10.1029/2024GL111902>, 2024.
- 738 Gorter, W., van Angelen, J. H., Lenaerts, J. T. M., and van den Broeke, M. R.: Present and future near-surface wind climate
739 of Greenland from high resolution regional climate modelling, *Clim Dyn*, 42, 1595–1611, [https://doi.org/10.1007/s00382-013-](https://doi.org/10.1007/s00382-013-1861-2)
740 1861-2, 2014.
- 741 Gutmann, E. D., Rasmussen, R. M., Liu, C., Ikeda, K., Bruyere, C. L., Done, J. M., Garrè, L., Friis-Hansen, P., and Veldore,
742 V.: Changes in Hurricanes from a 13-Yr Convection-Permitting Pseudo-Global Warming Simulation, *Journal of Climate*, 31,
743 3643–3657, <https://doi.org/10.1175/JCLI-D-17-0391.1>, 2018.
- 744 Hanna, E., Jónsson, T., Ólafsson, J., and Valdimarsson, H.: Icelandic Coastal Sea Surface Temperature Records Constructed:
745 Putting the Pulse on Air–Sea–Climate Interactions in the Northern North Atlantic. Part I: Comparison with HadISST1 Open-
746 Ocean Surface Temperatures and Preliminary Analysis of Long-Term Patterns and Anomalies of SSTs around Iceland, *Journal*
747 *of Climate*, 19, 5652–5666, <https://doi.org/10.1175/JCLI3933.1>, 2006.
- 748 Hanna, E., Huybrechts, P., Steffen, K., Cappelen, J., Huff, R., Shuman, C., Irvine-Fynn, T., Wise, S., and Griffiths, M.:
749 Increased Runoff from Melt from the Greenland Ice Sheet: A Response to Global Warming, *J. Climate*, 21, 331–341,
750 <https://doi.org/10.1175/2007JCLI1964.1>, 2008.
- 751 Hanna, E., Cappelen, J., Fettweis, X., Huybrechts, P., Luckman, A., and Ribergaard, M. H.: Hydrologic response of the
752 Greenland ice sheet: the role of oceanographic warming, *Hydrological Processes*, 23, 7–30, <https://doi.org/10.1002/hyp.7090>,
753 2009.
- 754 Hanna, E., Jones, J. M., Cappelen, J., Mernild, S. H., Wood, L., Steffen, K., and Huybrechts, P.: The influence of North Atlantic
755 atmospheric and oceanic forcing effects on 1900-2010 Greenland summer climate and ice melt/runoff, *Int. J. Climatol.*, 33,
756 862–880, <https://doi.org/10.1002/joc.3475>, 2013.
- 757 Hanna, E., Fettweis, X., Mernild, S. H., Cappelen, J., Ribergaard, M. H., Shuman, C. A., Steffen, K., Wood, L., and Mote, T.
758 L.: Atmospheric and oceanic climate forcing of the exceptional Greenland ice sheet surface melt in summer 2012, *International*
759 *Journal of Climatology*, 34, 1022–1037, <https://doi.org/10.1002/joc.3743>, 2014.
- 760 Hanna, E., Cropper, T. E., Jones, P. D., Scaife, A. A., and Allan, R.: Recent seasonal asymmetric changes in the NAO (a
761 marked summer decline and increased winter variability) and associated changes in the AO and Greenland Blocking Index,
762 *International Journal of Climatology*, 35, 2540–2554, <https://doi.org/10.1002/joc.4157>, 2015.
- 763 Hanna, E., Cropper, T. E., Hall, R. J., and Cappelen, J.: Greenland Blocking Index 1851-2015: a regional climate change
764 signal: Greenland Blocking Index 1851-2015, *Int. J. Climatol.*, 36, 4847–4861, <https://doi.org/10.1002/joc.4673>, 2016.
- 765 Hanna, E., Fettweis, X., and Hall, R. J.: Brief communication: Recent changes in summer Greenland blocking captured by
766 none of the CMIP5 models, *The Cryosphere*, 12, 3287–3292, <https://doi.org/10.5194/tc-12-3287-2018>, 2018a.
- 767 Hanna, E., Hall, R. J., Cropper, T. E., Ballinger, T. J., Wake, L., Mote, T., and Cappelen, J.: Greenland blocking index daily
768 series 1851–2015: Analysis of changes in extremes and links with North Atlantic and UK climate variability and change,
769 *International Journal of Climatology*, 38, 3546–3564, <https://doi.org/10.1002/joc.5516>, 2018b.

- 770 Hanna, E., Cappelen, J., Fettweis, X., Mernild, S. H., Mote, T. L., Mottram, R., Steffen, K., Ballinger, T. J., and Hall, R. J.:
771 Greenland surface air temperature changes from 1981 to 2019 and implications for ice-sheet melt and mass-balance change,
772 *International Journal of Climatology*, 41, E1336–E1352, <https://doi.org/10.1002/joc.6771>, 2021.
- 773 Hanna, E., Cropper, T. E., Hall, R. J., Combes, R. C., and Barriendos, M.: Extended North Atlantic Oscillation and Greenland
774 Blocking Indices 1800–2020 from New Meteorological Reanalysis, *Atmosphere*, 13, 436,
775 <https://doi.org/10.3390/atmos13030436>, 2022.
- 776 Hanna, E., Topál, D., Box, J. E., Buzzard, S., Christie, F. D. W., Hvidberg, C., Morlighem, M., De Santis, L., Silvano, A.,
777 Colleoni, F., Sasgen, I., Banwell, A. F., van den Broeke, M. R., DeConto, R., De Rydt, J., Goelzer, H., Gossart, A.,
778 Gudmundsson, G. H., Lindbäck, K., Miles, B., Mottram, R., Pattyn, F., Reese, R., Rignot, E., Srivastava, A., Sun, S., Toller,
779 J., Tuckett, P. A., and Ultee, L.: Short- and long-term variability of the Antarctic and Greenland ice sheets, *Nat Rev Earth*
780 *Environ*, 5, 193–210, <https://doi.org/10.1038/s43017-023-00509-7>, 2024.
- 781 Henderson, G. R., Barrett, B. S., Wachowicz, L. J., Mattingly, K. S., Preece, J. R., and Mote, T. L.: Local and Remote
782 Atmospheric Circulation Drivers of Arctic Change: A Review, *Frontiers in Earth Science*, 9,
783 <https://doi.org/10.3389/feart.2021.709896>, 2021.
- 784 Hermann, M., Papritz, L., and Wernli, H.: A Lagrangian analysis of the dynamical and thermodynamic drivers of large-scale
785 Greenland melt events during 1979–2017, *Weather and Climate Dynamics*, 1, 497–518, [https://doi.org/10.5194/wcd-1-497-](https://doi.org/10.5194/wcd-1-497-2020)
786 2020, 2020.
- 787 Hofer, S., Tedstone, A. J., Fettweis, X., and Bamber, J. L.: Decreasing cloud cover drives the recent mass loss on the Greenland
788 Ice Sheet, *Science Advances*, 3, e1700584, <https://doi.org/10.1126/sciadv.1700584>, 2017.
- 789 Horwath, M., Gutknecht, B. D., Cazenave, A., Palanisamy, H. K., Marti, F., Marzeion, B., Paul, F., Le Bris, R., Hogg, A. E.,
790 Ootaka, I., Shepherd, A., Döll, P., Cáceres, D., Müller Schmied, H., Johannessen, J. A., Nilsen, J. E. Ø., Raj, R. P., Forsberg,
791 R., Sandberg Sørensen, L., Barletta, V. R., Simonsen, S. B., Knudsen, P., Andersen, O. B., Rannald, H., Rose, S. K., Merchant,
792 C. J., Macintosh, C. R., von Schuckmann, K., Novotny, K., Groh, A., Restano, M., and Benveniste, J.: Global sea-level budget
793 and ocean-mass budget, with a focus on advanced data products and uncertainty characterisation, *Earth System Science Data*,
794 14, 411–447, <https://doi.org/10.5194/essd-14-411-2022>, 2022.
- 795 Hurrell, J. W., Hack, J. J., Shea, D., Caron, J. M., and Rosinski, J.: A New Sea Surface Temperature and Sea Ice Boundary
796 Dataset for the Community Atmosphere Model, *Journal of Climate*, 21, 5145–5153, <https://doi.org/10.1175/2008JCLI2292.1>,
797 2008.
- 798 Hurrell, James W., Phillips, Adam, and Shea, Dennis: Merged Hadley-OI sea surface temperature and sea ice concentration
799 data set, <https://doi.org/10.5065/R33V-SV91>, 2020.
- 800 Kawase, H., Yoshikane, T., Hara, M., Ailikun, B., Kimura, F., and Yasunari, T.: Downscaling of the Climatic Change in the
801 Mei-yu Rainband in East Asia by a Pseudo Climate Simulation Method, *SOLA*, 4, 73–76, [https://doi.org/10.2151/sola.2008-](https://doi.org/10.2151/sola.2008-019)
802 019, 2008.
- 803 Kay, J., Deser, C., Phillips, A., and Simpson, I.: CESM1 Large Ensemble Community Project,
804 <https://doi.org/10.5065/D6J101D1>, 2021.
- 805 Kay, J. E., Deser, C., Phillips, A., Mai, A., Hannay, C., Strand, G., Arblaster, J. M., Bates, S. C., Danabasoglu, G., Edwards,
806 J., Holland, M., Kushner, P., Lamarque, J.-F., Lawrence, D., Lindsay, K., Middleton, A., Munoz, E., Neale, R., Oleson, K.,
807 Polvani, L., and Vertenstein, M.: The Community Earth System Model (CESM) Large Ensemble Project: A Community

- 808 Resource for Studying Climate Change in the Presence of Internal Climate Variability, *Bulletin of the American*
809 *Meteorological Society*, 96, 1333–1349, <https://doi.org/10.1175/BAMS-D-13-00255.1>, 2015.
- 810 Khan, S. A., Aschwanden, A., Bjørk, A. A., Wahr, J., Kjeldsen, K. K., and Kjær, K. H.: Greenland ice sheet mass balance: a
811 review, *Rep. Prog. Phys.*, 78, 046801, <https://doi.org/10.1088/0034-4885/78/4/046801>, 2015.
- 812 Kimura, F. and Kitoh, A.: Downscaling by pseudo global warming method, *The Final Report of ICCAP*, 4346, 2007.
- 813 Kjeldsen, K. K., Korsgaard, N. J., Bjørk, A. A., Khan, S. A., Box, J. E., Funder, S., Larsen, N. K., Bamber, J. L., Colgan, W.,
814 van den Broeke, M., Siggaard-Andersen, M.-L., Nuth, C., Schomacker, A., Andresen, C. S., Willerslev, E., and Kjær, K. H.:
815 Spatial and temporal distribution of mass loss from the Greenland Ice Sheet since AD 1900, *Nature*, 528, 396–400,
816 <https://doi.org/10.1038/nature16183>, 2015.
- 817 Kornhuber, K. and Tamarin-Brodsky, T.: Future Changes in Northern Hemisphere Summer Weather Persistence Linked to
818 Projected Arctic Warming, *Geophysical Research Letters*, 48, e2020GL091603, <https://doi.org/10.1029/2020GL091603>,
819 2021.
- 820 Lackmann, G. M.: Hurricane Sandy before 1900 and after 2100, *Bull. Amer. Meteor. Soc.*, 96, 547–560,
821 <https://doi.org/10.1175/BAMS-D-14-00123.1>, 2015.
- 822 Lee, S. H. and Polvani, L. M.: Increasing Frequency and Persistence of the Summertime Greenland High Regime Not Captured
823 by a Seasonal Prediction Model Very Large Ensemble, *Geophysical Research Letters*, 53, e2025GL119421,
824 <https://doi.org/10.1029/2025GL119421>, 2026.
- 825 Lefebvre, F., Fettweis, X., Gallée, H., Van Ypersele, J.-P., Marbaix, P., Greuell, W., and Calanca, P.: Evaluation of a high-
826 resolution regional climate simulation over Greenland, *Climate Dynamics*, 25, 99–116, <https://doi.org/10.1007/s00382-005-0005-8>, 2005.
- 828 Lenaerts, J. T. M., Medley, B., van den Broeke, M. R., and Wouters, B.: Observing and Modeling Ice Sheet Surface Mass
829 Balance, *Reviews of Geophysics*, 57, 376–420, <https://doi.org/10.1029/2018RG000622>, 2019.
- 830 Liu, J., Chen, Z., Francis, J., Song, M., Mote, T., and Hu, Y.: Has Arctic Sea Ice Loss Contributed to Increased Surface Melting
831 of the Greenland Ice Sheet?, *J. Climate*, 29, 3373–3386, <https://doi.org/10.1175/JCLI-D-15-0391.1>, 2016.
- 832 Lloyd, E. A. and Oreskes, N.: Climate Change Attribution: When Is It Appropriate to Accept New Methods?, *Earth’s Future*,
833 6, 311–325, <https://doi.org/10.1002/2017EF000665>, 2018.
- 834 Luu, L. N., Hanna, E., de Alwis Pitts, D., Maddison, J., Screen, J. A., Catto, J. L., and Fettweis, X.: Greenland summer blocking
835 characteristics: an evaluation of a high-resolution multi-model ensemble, *Clim Dyn*, 62, 10503–10523,
836 <https://doi.org/10.1007/s00382-024-07453-2>, 2024.
- 837 Mallard, M. S., Lackmann, G. M., Aiyyer, A., and Hill, K.: Atlantic Hurricanes and Climate Change. Part I: Experimental
838 Design and Isolation of Thermodynamic Effects, *Journal of Climate*, 26, 4876–4893, <https://doi.org/10.1175/JCLI-D-12-00182.1>, 2013.
- 840 Mankoff, K. D., Colgan, W., Solgaard, A., Karlsson, N. B., Ahlstrøm, A. P., As, D. V., Box, J. E., Khan, S. A., Kjeldsen, K.
841 K., Mouginot, J., and Fausto, R. S.: Greenland Ice Sheet solid ice discharge from 1986 through 2017, *Earth System Science*
842 *Data*, 11, 769–786, <https://doi.org/10.5194/essd-11-769-2019>, 2019.

- 843 Mattingly, K. S., Ramseyer, C. A., Rosen, J. J., Mote, T. L., and Muthyala, R.: Increasing water vapor transport to the
844 Greenland Ice Sheet revealed using self-organizing maps, *Geophysical Research Letters*, 43, 9250–9258,
845 <https://doi.org/10.1002/2016GL070424>, 2016.
- 846 Mattingly, K. S., Mote, T. L., and Fettweis, X.: Atmospheric River Impacts on Greenland Ice Sheet Surface Mass Balance,
847 *Journal of Geophysical Research: Atmospheres*, 123, 8538–8560, <https://doi.org/10.1029/2018JD028714>, 2018.
- 848 Meese, D. A., Gow, A. J., Grootes, P., Mayewski, P. A., Ram, M., Stuiver, M., Taylor, K. C., Waddington, E. D., and Zielinski,
849 G. A.: The Accumulation Record from the GISP2 Core as an Indicator of Climate Change Throughout the Holocene, *Science*,
850 266, 1680–1682, 1994.
- 851 Mote, T. L.: Mid-tropospheric circulation and surface melt on the Greenland ice sheet. Part I: atmospheric teleconnections,
852 *International Journal of Climatology*, 18, 111–129, [https://doi.org/10.1002/\(SICI\)1097-0088\(199802\)18:2%253C111::AID-
853 JOC227%253E3.0.CO;2-X](https://doi.org/10.1002/(SICI)1097-0088(199802)18:2%253C111::AID-JOC227%253E3.0.CO;2-X), 1998.
- 854 Mote, T. L.: Greenland surface melt trends 1973–2007: Evidence of a large increase in 2007, *Geophysical Research Letters*,
855 34, <https://doi.org/10.1029/2007GL031976>, 2007.
- 856 Mouginit, J., Rignot, E., Bjørk, A. A., van den Broeke, M. R., Millan, R., Morlighem, M., Noël, B., Scheuchl, B., and Wood,
857 M.: Forty-six years of Greenland Ice Sheet mass balance from 1972 to 2018, *PNAS*, 116, 9239–9244,
858 <https://doi.org/10.1073/pnas.1904242116>, 2019.
- 859 Neff, W., Compo, G. P., Martin Ralph, F., and Shupe, M. D.: Continental heat anomalies and the extreme melting of the
860 Greenland ice surface in 2012 and 1889: Melting of Greenland in 1889 and 2012, *J. Geophys. Res. Atmos.*, 119, 6520–6536,
861 <https://doi.org/10.1002/2014JD021470>, 2014.
- 862 Nghiem, S. V., Hall, D. K., Mote, T. L., Tedesco, M., Albert, M. R., Keegan, K., Shuman, C. A., DiGirolamo, N. E., and
863 Neumann, G.: The extreme melt across the Greenland ice sheet in 2012, *Geophysical Research Letters*, 39,
864 <https://doi.org/10.1029/2012GL053611>, 2012.
- 865 Noël, B., Fettweis, X., van de Berg, W. J., van den Broeke, M. R., and Erpicum, M.: Sensitivity of Greenland Ice Sheet surface
866 mass balance to perturbations in sea surface temperature and sea ice cover: a study with the regional climate model MAR, *The
867 Cryosphere*, 8, 1871–1883, <https://doi.org/10.5194/tc-8-1871-2014>, 2014.
- 868 Noël, B., van de Berg, W. J., Lhermitte, S., Wouters, B., Machguth, H., Howat, I., Citterio, M., Moholdt, G., Lenaerts, J. T.
869 M., and van den Broeke, M. R.: A tipping point in refreezing accelerates mass loss of Greenland’s glaciers and ice caps, *Nat
870 Commun*, 8, 14730, <https://doi.org/10.1038/ncomms14730>, 2017.
- 871 Noël, B., Berg, W. J. van de, Lhermitte, S., and van den Broeke, M. R.: Rapid ablation zone expansion amplifies north
872 Greenland mass loss, *Science Advances*, 5, eaaw0123, <https://doi.org/10.1126/sciadv.aaw0123>, 2019.
- 873 Noël, B., van Kampenhout, L., Lenaerts, J. T. M., van de Berg, W. J., and van den Broeke, M. R.: A 21st Century Warming
874 Threshold for Sustained Greenland Ice Sheet Mass Loss, *Geophysical Research Letters*, 48, e2020GL090471,
875 <https://doi.org/10.1029/2020GL090471>, 2021.
- 876 Ogi, M. and Wallace, J. M.: Summer minimum Arctic sea ice extent and the associated summer atmospheric circulation,
877 *Geophysical Research Letters*, 34, <https://doi.org/10.1029/2007GL029897>, 2007.

- 878 Orsi, A. J., Kawamura, K., Masson-Delmotte, V., Fettweis, X., Box, J. E., Dahl-Jensen, D., Clow, G. D., Landais, A., and
879 Severinghaus, J. P.: The recent warming trend in North Greenland, *Geophysical Research Letters*, 44, 6235–6243,
880 <https://doi.org/10.1002/2016GL072212>, 2017.
- 881 Otosaka, I. N., Shepherd, A., Ivins, E. R., Schlegel, N.-J., Amory, C., van den Broeke, M. R., Horwath, M., Joughin, I., King,
882 M. D., Krinner, G., Nowicki, S., Payne, A. J., Rignot, E., Scambos, T., Simon, K. M., Smith, B. E., Sørensen, L. S., Velicogna,
883 I., Whitehouse, P. L., A. G., Agosta, C., Ahlström, A. P., Blazquez, A., Colgan, W., Engdahl, M. E., Fettweis, X., Forsberg,
884 R., Gallée, H., Gardner, A., Gilbert, L., Gourmelen, N., Groh, A., Gunter, B. C., Harig, C., Helm, V., Khan, S. A., Kittel, C.,
885 Konrad, H., Langen, P. L., Lecavalier, B. S., Liang, C.-C., Loomis, B. D., McMillan, M., Melini, D., Mernild, S. H., Mottram,
886 R., Mougnot, J., Nilsson, J., Noël, B., Pattle, M. E., Peltier, W. R., Pie, N., Roca, M., Sasgen, I., Save, H. V., Seo, K.-W.,
887 Scheuchl, B., Schrama, E. J. O., Schröder, L., Simonsen, S. B., Slater, T., Spada, G., Sutterley, T. C., Vishwakarma, B. D.,
888 van Wessem, J. M., Wiese, D., van der Wal, W., and Wouters, B.: Mass balance of the Greenland and Antarctic ice sheets
889 from 1992 to 2020, *Earth System Science Data*, 15, 1597–1616, <https://doi.org/10.5194/essd-15-1597-2023>, 2023.
- 890 Overland, J. E., Francis, J. A., Hanna, E., and Wang, M.: The recent shift in early summer Arctic atmospheric circulation,
891 *Geophysical Research Letters*, 39, L19804, <https://doi.org/10.1029/2012GL053268>, 2012.
- 892 Pedersen, R. A. and Christensen, J. H.: Attributing Greenland Warming Patterns to Regional Arctic Sea Ice Loss, *Geophysical*
893 *Research Letters*, 46, 10495–10503, <https://doi.org/10.1029/2019GL083828>, 2019.
- 894 Pithan, F. and Mauritsen, T.: Arctic amplification dominated by temperature feedbacks in contemporary climate models,
895 *Nature Geosci*, 7, 181–184, <https://doi.org/10.1038/ngeo2071>, 2014.
- 896 Preece, J., Alexander, P., Mote, T., Kooperman, G., Fettweis, X., and Tedesco, M.: Modèle Atmosphérique Régional (MAR)
897 version 3.12 regional climate model pseudo-global warming experiment output, 2000-2019, Greenland domain, 20 kilometer
898 (km) horizontal resolution., <https://doi.org/10.18739/A2TT4FV6W>, 2023a.
- 899 Preece, J. R., Wachowicz, L. J., Mote, T. L., Tedesco, M., and Fettweis, X.: Summer Greenland Blocking Diversity and Its
900 Impact on the Surface Mass Balance of the Greenland Ice Sheet, *Journal of Geophysical Research: Atmospheres*, 127,
901 e2021JD035489, <https://doi.org/10.1029/2021JD035489>, 2022.
- 902 Preece, J. R., Mote, T. L., Cohen, J., Wachowicz, L. J., Knox, J. A., Tedesco, M., and Kooperman, G. J.: Summer atmospheric
903 circulation over Greenland in response to Arctic amplification and diminished spring snow cover, *Nat Commun*, 14, 3759,
904 <https://doi.org/10.1038/s41467-023-39466-6>, 2023b.
- 905 Rantanen, M., Karpechko, A. Y., Lipponen, A., Nordling, K., Hyvärinen, O., Ruosteenoja, K., Vihma, T., and Laaksonen, A.:
906 The Arctic has warmed nearly four times faster than the globe since 1979, *Commun Earth Environ*, 3, 1–10,
907 <https://doi.org/10.1038/s43247-022-00498-3>, 2022.
- 908 Rasmussen, K. L., Prein, A. F., Rasmussen, R. M., Ikeda, K., and Liu, C.: Changes in the convective population and
909 thermodynamic environments in convection-permitting regional climate simulations over the United States, *Clim Dyn*, 55,
910 383–408, <https://doi.org/10.1007/s00382-017-4000-7>, 2020.
- 911 Rasmussen, R., Liu, C., Ikeda, K., Gochis, D., Yates, D., Chen, F., Tewari, M., Barlage, M., Dudhia, J., Yu, W., Miller, K.,
912 Arsenault, K., Grubišić, V., Thompson, G., and Gutmann, E.: High-Resolution Coupled Climate Runoff Simulations of
913 Seasonal Snowfall over Colorado: A Process Study of Current and Warmer Climate, *J. Climate*, 24, 3015–3048,
914 <https://doi.org/10.1175/2010JCLI3985.1>, 2011.
- 915 Rennermalm, A. K., Smith, L. C., Stroeve, J. C., and Chu, V. W.: Does sea ice influence Greenland ice sheet surface-melt?,
916 *Environ. Res. Lett.*, 4, 024011, <https://doi.org/10.1088/1748-9326/4/2/024011>, 2009.

- 917 Rogers, J. C., Bathke, D. J., Mosley-Thompson, E., and Wang, S.-H.: Atmospheric circulation and cyclone frequency
918 variations linked to the primary modes of Greenland snow accumulation, *Geophysical Research Letters*, 31,
919 <https://doi.org/10.1029/2004GL021048>, 2004.
- 920 Schär, C., Frei, C., Lüthi, D., and Davies, H. C.: Surrogate climate-change scenarios for regional climate models, *Geophys.*
921 *Res. Lett.*, 23, 669–672, <https://doi.org/10.1029/96GL00265>, 1996.
- 922 Schoof, C.: Ice-sheet acceleration driven by melt supply variability, *Nature*, 468, 803–806,
923 <https://doi.org/10.1038/nature09618>, 2010.
- 924 Schuenemann, K. C., Cassano, J. J., and Finnis, J.: Synoptic Forcing of Precipitation over Greenland: Climatology for 1961–
925 99, *Journal of Hydrometeorology*, 10, 60–78, <https://doi.org/10.1175/2008JHM1014.1>, 2009.
- 926 Screen, J. A.: Influence of Arctic sea ice on European summer precipitation, *Environ. Res. Lett.*, 8, 044015,
927 <https://doi.org/10.1088/1748-9326/8/4/044015>, 2013.
- 928 Screen, J. A.: Far-flung effects of Arctic warming, *Nature Geosci*, 10, 253–254, <https://doi.org/10.1038/ngeo2924>, 2017.
- 929 Screen, J. A. and Simmonds, I.: The central role of diminishing sea ice in recent Arctic temperature amplification, *Nature*, 464,
930 1334–1337, <https://doi.org/10.1038/nature09051>, 2010.
- 931 Sellevold, R., Lenaerts, J. T. M., and Vizcaino, M.: Influence of Arctic sea-ice loss on the Greenland ice sheet climate, *Clim*
932 *Dyn*, 58, 179–193, <https://doi.org/10.1007/s00382-021-05897-4>, 2022.
- 933 Serreze, M. C. and Barry, R. G.: Processes and impacts of Arctic amplification: A research synthesis, *Global and Planetary*
934 *Change*, 77, 85–96, <https://doi.org/10.1016/j.gloplacha.2011.03.004>, 2011.
- 935 Shea, D., Hurrell, J., and Phillips, A.: Merged Hadley-OI sea surface temperature and sea ice concentration data set,
936 <https://doi.org/10.5065/R33V-SV91>, 2020.
- 937 Smith, B., Fricker, H. A., Gardner, A. S., Medley, B., Nilsson, J., Paolo, F. S., Holschuh, N., Adusumilli, S., Brunt, K., Csatho,
938 B., Harbeck, K., Markus, T., Neumann, T., Siegfried, M. R., and Zwally, H. J.: Pervasive ice sheet mass loss reflects competing
939 ocean and atmosphere processes, *Science*, 368, 1239–1242, <https://doi.org/10.1126/science.aaz5845>, 2020.
- 940 Stroeve, J. C., Mioduszewski, J. R., Rennermalm, A., Boisvert, L. N., Tedesco, M., and Robinson, D.: Investigating the local-
941 scale influence of sea ice on Greenland surface melt, *The Cryosphere*, 11, 2363–2381, [https://doi.org/10.5194/tc-11-2363-](https://doi.org/10.5194/tc-11-2363-2017)
942 2017, 2017.
- 943 Tedesco, M. and Fettweis, X.: Unprecedented atmospheric conditions (1948–2019) drive the 2019 exceptional melting season
944 over the Greenland ice sheet, *Cryosphere*, 14, 1209–1223, <https://doi.org/10.5194/tc-14-1209-2020>, 2020.
- 945 Tedesco, M., Mote, T., Fettweis, X., Hanna, E., Jeyaratnam, J., Booth, J. F., Datta, R., and Briggs, K.: Arctic cut-off high
946 drives the poleward shift of a new Greenland melting record, *Nat Commun*, 7, 11723, <https://doi.org/10.1038/ncomms11723>,
947 2016.
- 948 The GlaMBIE Team, Zemp, M., Jakob, L., Dussillant, I., Nussbaumer, S. U., Gourmelen, N., Dubber, S., A, G., Abdullahi,
949 S., Andreassen, L. M., Berthier, E., Bhattacharya, A., Blazquez, A., Boehm Vock, L. F., Bolch, T., Box, J., Braun, M. H.,
950 Brun, F., Cicero, E., Colgan, W., Eckert, N., Farinotti, D., Florentine, C., Floricioiu, D., Gardner, A., Harig, C., Hassan, J.,
951 Hugonnet, R., Huss, M., Jóhannesson, T., Liang, C.-C. A., Ke, C.-Q., Khan, S. A., King, O., Kneib, M., Krieger, L., Maussion,
952 F., Mattea, E., McNabb, R., Menounos, B., Miles, E., Moholdt, G., Nilsson, J., Pálsson, F., Pfeffer, J., Piermattei, L., Plummer,

- 953 S., Richter, A., Sasgen, I., Schuster, L., Seehaus, T., Shen, X., Sommer, C., Sutterley, T., Treichler, D., Velicogna, I., Wouters,
954 B., Zekollari, H., Zheng, W., and The GlaMBIE Team: Community estimate of global glacier mass changes from 2000 to
955 2023, *Nature*, 639, 382–388, <https://doi.org/10.1038/s41586-024-08545-z>, 2025.
- 956 The IMBIE team, Shepherd, A., Ivins, E., Rignot, E., Smith, B., van den Broeke, M., Velicogna, I., Whitehouse, P., Briggs,
957 K., Joughin, I., Krinner, G., Nowicki, S., Payne, T., Scambos, T., Schlegel, N., A. G., Agosta, C., Ahlstrøm, A., Babonis, G.,
958 Barletta, V., Blazquez, A., Bonin, J., Csatho, B., Cullather, R., Felikson, D., Fettweis, X., Forsberg, R., Gallee, H., Gardner,
959 A., Gilbert, L., Groh, A., Gunter, B., Hanna, E., Harig, C., Helm, V., Horvath, A., Horwath, M., Khan, S., Kjeldsen, K. K.,
960 Konrad, H., Langen, P., Lecavalier, B., Loomis, B., Luthcke, S., McMillan, M., Melini, D., Mernild, S., Mohajerani, Y., Moore,
961 P., Mouginot, J., Moyano, G., Muir, A., Nagler, T., Nield, G., Nilsson, J., Noel, B., Otosaka, I., Pattle, M. E., Peltier, W. R.,
962 Pie, N., Rietbroek, R., Rott, H., Sandberg-Sørensen, L., Sasgen, I., Save, H., Scheuchl, B., Schrama, E., Schröder, L., Seo, K.-
963 W., Simonsen, S., Slater, T., Spada, G., Sutterley, T., Talpe, M., Tarasov, L., van de Berg, W. J., van der Wal, W., van Wessem,
964 M., Vishwakarma, B. D., Wiese, D., and Wouters, B.: Mass balance of the Antarctic Ice Sheet from 1992 to 2017, *Nature*,
965 558, 219–222, <https://doi.org/10.1038/s41586-018-0179-y>, 2018.
- 966 The IMBIE Team, Shepherd, A., Ivins, E., Rignot, E., Smith, B., van den Broeke, M., Velicogna, I., Whitehouse, P., Briggs,
967 K., Joughin, I., Krinner, G., Nowicki, S., Payne, T., Scambos, T., Schlegel, N., A. G., Agosta, C., Ahlstrøm, A., Babonis, G.,
968 Barletta, V. R., Bjørk, A. A., Blazquez, A., Bonin, J., Colgan, W., Csatho, B., Cullather, R., Engdahl, M. E., Felikson, D.,
969 Fettweis, X., Forsberg, R., Hogg, A. E., Gallee, H., Gardner, A., Gilbert, L., Gourmelen, N., Groh, A., Gunter, B., Hanna, E.,
970 Harig, C., Helm, V., Horvath, A., Horwath, M., Khan, S., Kjeldsen, K. K., Konrad, H., Langen, P. L., Lecavalier, B., Loomis,
971 B., Luthcke, S., McMillan, M., Melini, D., Mernild, S., Mohajerani, Y., Moore, P., Mottram, R., Mouginot, J., Moyano, G.,
972 Muir, A., Nagler, T., Nield, G., Nilsson, J., Noël, B., Otosaka, I., Pattle, M. E., Peltier, W. R., Pie, N., Rietbroek, R., Rott, H.,
973 Sandberg Sørensen, L., Sasgen, I., Save, H., Scheuchl, B., Schrama, E., Schröder, L., Seo, K.-W., Simonsen, S. B., Slater, T.,
974 Spada, G., Sutterley, T., Talpe, M., Tarasov, L., van de Berg, W. J., van der Wal, W., van Wessem, M., Vishwakarma, B. D.,
975 Wiese, D., Wilton, D., Wagner, T., Wouters, B., and Wuite, J.: Mass balance of the Greenland Ice Sheet from 1992 to 2018,
976 *Nature*, 579, 233–239, <https://doi.org/10.1038/s41586-019-1855-2>, 2020.
- 977 Topál, D., Ding, Q., Ballinger, T. J., Hanna, E., Fettweis, X., Li, Z., and Pieczka, I.: Discrepancies between observations and
978 climate models of large-scale wind-driven Greenland melt influence sea-level rise projections, *Nat Commun*, 13,
979 <https://doi.org/10.1038/s41467-022-34414-2>, 2022.
- 980 Trenberth, K. E.: Changes in precipitation with climate change, *Climate Research*, 47, 123–138, 2011.
- 981 Trenberth, K. E., Fasullo, J. T., and Shepherd, T. G.: Attribution of climate extreme events, *Nature Clim Change*, 5, 725–730,
982 <https://doi.org/10.1038/nclimate2657>, 2015.
- 983 Vavrus, S. J., Wang, F., Martin, J. E., Francis, J. A., Peings, Y., and Cattiaux, J.: Changes in North American Atmospheric
984 Circulation and Extreme Weather: Influence of Arctic Amplification and Northern Hemisphere Snow Cover, *J. Climate*, 30,
985 4317–4333, <https://doi.org/10.1175/JCLI-D-16-0762.1>, 2017.
- 986 Velicogna, I., Mohajerani, Y., A. G., Landerer, F., Mouginot, J., Noel, B., Rignot, E., Sutterley, T., van den Broeke, M., van
987 Wessem, M., and Wiese, D.: Continuity of Ice Sheet Mass Loss in Greenland and Antarctica From the GRACE and GRACE
988 Follow-On Missions, *Geophysical Research Letters*, 47, e2020GL087291, <https://doi.org/10.1029/2020GL087291>, 2020.
- 989 Wang, S., Ma, X., Zhou, S., Wu, L., Wang, H., Tang, Z., Xu, G., Jing, Z., Chen, Z., and Gan, B.: Extreme atmospheric rivers
990 in a warming climate, *Nat Commun*, 14, 3219, <https://doi.org/10.1038/s41467-023-38980-x>, 2023.
- 991 Wang, W., Zender, C. S., and As, D. van: Temporal Characteristics of Cloud Radiative Effects on the Greenland Ice Sheet:
992 Discoveries From Multiyear Automatic Weather Station Measurements, *Journal of Geophysical Research: Atmospheres*, 123,
993 11,348–11,361, <https://doi.org/10.1029/2018JD028540>, 2018.

- 994 Wang, W., Zender, C. S., As, D. van, and Miller, N. B.: Spatial Distribution of Melt Season Cloud Radiative Effects Over
995 Greenland: Evaluating Satellite Observations, Reanalyses, and Model Simulations Against In Situ Measurements, *Journal of*
996 *Geophysical Research: Atmospheres*, 124, 57–71, <https://doi.org/10.1029/2018JD028919>, 2019.
- 997 Wilcoxon, F.: Individual Comparisons by Ranking Methods, *Biometrics Bulletin*, 1, 80–83, <https://doi.org/10.2307/3001968>,
998 1945.
- 999 Woollings, T., Barriopedro, D., Methven, J., Son, S.-W., Martius, O., Harvey, B., Sillmann, J., Lupo, A. R., and Seneviratne,
1000 S.: Blocking and its Response to Climate Change, *Curr Clim Change Rep*, 4, 287–300, [https://doi.org/10.1007/s40641-018-](https://doi.org/10.1007/s40641-018-0108-z)
1001 [0108-z](https://doi.org/10.1007/s40641-018-0108-z), 2018.
- 1002 Wu, B., Zhang, R., D’Arrigo, R., and Su, J.: On the Relationship between Winter Sea Ice and Summer Atmospheric Circulation
1003 over Eurasia, *J. Climate*, 26, 5523–5536, <https://doi.org/10.1175/JCLI-D-12-00524.1>, 2013.
- 1004 Yang, C., Leonelli, F. E., Marullo, S., Artale, V., Beggs, H., Nardelli, B. B., Chin, T. M., Toma, V. D., Good, S., Huang, B.,
1005 Merchant, C. J., Sakurai, T., Santoleri, R., Vazquez-Cuervo, J., Zhang, H.-M., and Pisano, A.: Sea Surface Temperature
1006 Intercomparison in the Framework of the Copernicus Climate Change Service (C3S), *Journal of Climate*, 34, 5257–5283,
1007 <https://doi.org/10.1175/JCLI-D-20-0793.1>, 2021.
- 1008